Regulation of Tubulin dynamics by the +Tip tracking protein Mal3

Amédée des Georges

Hughes Hall, University of Cambridge

Thesis submitted to the University of Cambridge
for the degree of Doctor of Philosophy, July 2008

Declaration

This dissertation is the result of my own work and includes nothing which is the outcome of work done in collaboration except where specifically indicated in the text. There are no parts of this thesis in any form which have been submitted for any other qualification. Permission is granted to copy the information contained herein for the purpose of private study, but not for publication.This thesis does not exceed the word limit prescribed by the Degree Committee of Biology.

Amédée des Georges

Acknoledgement

The work presented in this thesis was carried out at the MRC Laboratory of Molecular Biology, Cambridge, under the supervision of Linda Amos and Jan Löwe. I am sincerely grateful for having been given the opportunity to work with them and to benefit from their profound scientific insight and the motivating environment of their laboratory. I would especially like to thank Linda for giving me such an interesting project and the total freedom to pursue it in whatever direction I wished. I may not always have taken the path of least resistance but the experience has greatly strengthened my ability to do independent research and will be invaluable in future. Linda has also spent an enormous amount of time analysing a large number of EM micrographs and diffraction patterns and her insight has been crucial for the culmination of this project. I wish to thank Jan for his astute advice, invaluable help and the motivation he has provided, and to thank both Linda and Jan for being there when I needed them and always being so generous with their time.

I would like to thank Rob Cross for funding my PhD, and for the many experiments we ran at the Marie Curie research institute. He has given me constant support, for which I am truly grateful. In particular I owe thanks to Miho Katsuki and Doug Drummond for all what we have done together on this project. Many experiments would not have been possible without them.

I would also like to thank John Kilmartin for helping me set up the protein A immunoprecipitation experiment and for providing me with the necessary tools to carry it out. I also wish to thank Paul Conduit for his help with all technical aspects of it.
I wish to thank Daniel Schlieper, Harry Low, Jakob Møller-Jensen, Fusinita van den Ent and Thomas Leonard for their more than useful advice on cloning and protein purification and Daniel Trambaiolo for his technical help in obtaining the mal3 CH domain crystal structure.

I also owe thanks to Juan Fan, Harry Low, Chris Mercogliano and Jeanne Salje for always being there when I needed advice on using the electron microscope.

I would particularly like to thank Anne-Laure for her constant support, interest and curiosity over the last three years.

Finally I would especially like to thank everyone in Linda and Jan's laboratories for the fruitful scientific discussions that we have had over lunch and coffee and yet more for having been great friends and making these few years in Cambridge truly memorable.

Regulation of Tubulin dynamics by the +Tip tracking protein Mal3

Abstract

The Microtubule (MT) network is a central component of the eukaryotic cell cytoskeleton. In the fission yeast S. pombe, a complex of three proteins specifically tracks MT +ends and stabilizes MTs in the cell. It is composed of the proteins Mal3, Tip1 and Tea2. Mal3, the S. pombe homologue of EB1, is a highly conserved ubiquitous protein found to be at the centre of many MT related processes. Tip1 is a CLIP170 homologue and Tea2 a kinesin-like motor protein. The mechanism by which they target the growing end of MTs and stabilize them is still unknown. A combination of biochemistry, electron microscopy and crystallography were used in an attempt to get a more precise understanding of the MT stabilization by this +Tip complex. Protein-A pull-down of the endogenous complex and analysis of its constituents by mass spectrometry revealed that Tea2 and Tip1 form a tight stoichiometric complex, making a much more labile interaction with Mal3. Biochemical experiments, light scattering and DIC microscopy demonstrate that Mal3 stabilizes the MT structure in a stoichiometric fashion by suppressing catastrophe events. 3D helical reconstruction of electron micrographs of Mal3 bound to the MT show that it most probably stabilizes the MT structure by bridging protofilaments together. Deletion mutant analysis suggests that contact with one of the protofilaments is via an interaction between the charged tails of tubulin and Mal3. Mal3 MT binding domain structure was solved by X-ray crystallography so that eventually it may be docked into a higher resolution electron microscopy map to provide a more precise structural insight on how Mal3 stabilizes the MT lattice. The EM analysis also shows that Mal3 regulates MT structure in vitro by restraining their protofilament number to 13, which is the number always found in vivo, and by driving the assembly of MTs with a high proportion of A-lattice. It is the first time that a protein is found to promote formation of A-lattice MTs. The fact that EB1 is such a ubiquitous protein reopens the question of MT structure in cells and has important implications for in vivo MT dynamics.

Table of Contents

Publications..... VI

Abbreviations..... VII

Chapter 1. Introduction..... 1

The Microtubule cytoskeleton and its structure 1
Principles of dynamic instability 5
Microtubule polarity and end structure: physiological importance 6
3 classes of +end binding proteins 7
A tip-tracking complex required for *S. pombe* cell polarity maintenance 10

Chapter 2: Isolating a +Tip tracking complex by protein-A pull down in *S. pombe*..... 13

Stategy 13
Methods 15
Schizosaccharomyces pombe strains 15
PCR amplification of the protein A cassette 15
Transformation of S. pombe and selection of G418-resistant clones
Screening transformants for homologous integration by PCR 16
Backcrossing 17
Western blot 18
Purification of the +Tip Complex for Mass Spectrometry Analysis
Mass spectrometry 19
Results 20
Mass spectrometry analysis 20
Affinity purification of Tea2-prA and Tip1-prA by IgG-Sepharose chromatography 21

Chapter 3: Expression and purification of Mal3, Tip1 and Tea2 from *E. coli*..... 22

Strategy 22
Methods 23
Preparation of a S. pombe cDNA library 23
Oligonucleotide synthesis 23
Gene amplification by polymerase chain reaction (PCR) 24
PCR purification 25

DNA restriction endonuclease digest 25
Vector preparation 25
Agarose gel electrophoresis 25
DNA gel extraction 26
DNA insertion and ligation 26
***E.coli* transformation into cloning strains** 26
Plasmid amplification and purification 27
DNA sequencing 27
Culturing of *E. coli* clones 27
Expression of His-tagged protein constructs 27
Purification of His-tagged proteins 28
Expression of GST-tagged protein constructs 29
Purification of GST-tagged proteins 29
Results 30
Expression and purification of His tagged Mal3 and Tip1 protein constructs 30
Expression and purification of GST tagged Tip1 protein constructs
Kinesin expression and purification 32

Chapter 4: Characterisation of the +Tips - microtubule interaction 33

Strategy 33
Methods 34
***S. pombe* tubulin expression & purification** 34
Pig brain tubulin purification 34
MT Pelleting assays 35
Results 36
Mal3 binds to MTs in a one to one ratio to tubulin dimers. 36
Mal3 binds tighter to co-polymerised MTs 37
Does Tip1 interact with MTs? 39
Tea2 interacts with MTs and competes with Mal3 40

Chapter 5: Measuring +Tips effect on MT dynamics by light scattering and DIC microscopy 41

Strategy 41
Methods 41
Light scattering 41
Assay of assembly dynamics by VE-DIC 42
Results 43
Light Scattering assembly assay using Mal3 constructs 43
Assays of assembly dynamics by VE-DIC 45

Chapter 6: Decorating MTs with Mal3 monomer and studying the complex by electron microscopy.....46

Strategy 46
Helical symmetry 46
Methods 47
Negative staining of Mal3 bound to MTs 47
Kinesin decoration 47
Electron cryo-microscopy of Mal3-MT 48
Image analysis 48
Results 48
Negative stain study of Mal3dimers and monomers bound to MTs. 48
Finding the right specimen for helical 3D image reconstruction 50
Effect of DMSO 50
MT concentration on the grid 50
Looking for 15 pf MTs with helical symmetry 51
13-protofilament MTs with mixed lattices 52
3D reconstruction of a 13 pf A-lattice MT decorated with Mal3 56

Chapter 7: Cross-linking experiment..... 59

Strategy 59
Method 60
Results 60

Chapter 8: Mal3 X-ray crystallographic Study.....63

Strategy 63
Methods 63
Results 64

Chapter 9: Discussion and future directions..... 67

References..... 73

des Georges, A. Katsuki, M., Drummond, D., Osei, M., Cross, R.A. and Amos, L.A. Mal3, the S. pombe homologue of EB1, changes the microtubule lattice. *Nature Structural and Molecular Biology - in press*

aa	amino acid(s)
AMPPNP	Adenyl-5'-yl imidodiphosphate
ATP	Adenosine triphosphate
bp	base pair
BCA	bicinchoninic acid
BSA	bovine serum albumin
CCD	Charge-coupled device
ddw	double distilled/MilliQ water
DIC	differential interference contrast microscopy
DNA	Deoxyribonucleic acid
DNase	deoxyribonuclease
EDC or EDAC	1-ethyl-3-(3-dimethylaminopropyl) carbodiimide hydrochloride
EDTA	ethylenediaminetetraacetic acid
EGTA	ethylene glycol tetraacetic acid
EM	electron microscopy
DMSO	dimethyl sulphoxide
DTT	dithiothreitol
EM	electron microscopy
γ–TuRC	gamma-Tubulin Ring Complex
GDP	guanosine 5′-diphosphate
GMPCPP	guanylyl 5′-(α β-methylene)diphosphate
GTP	guanosine 5′-triphosphate
HCl	Hydrogen Chloride
hr(s)	hour(s)
IPTG	isopropyl-beta-D-thiogalactopyranoside
Da	Dalton(s)
kDa	kiloDalton(s)
LiOAc	Lithium Acetate
MALDI	Matrix-assisted laser desorption/ionization
MAP	microtubule associated protein
min	minutes
ml	millilitre
MRC	Medical Research Council
MT	microtubule
MTOC	Microtubule Organising Centre
MW	molecular weight

NCBI	National Center for Biotechnology Information
ng	nanograms
nmoles	nanomoles
PAGE	polyacrylamide gel electrophoresis
PBS	Phosphate buffered saline
PCR	Polymerase Chain Reaction
PEG	polyethylene glycol
Pi	phosphate
PIPES	piperazine-N,N'-bis(2-ethanesulfonic acid)
PMSF	phenylmethanesulphonylfluoride
prA	protein A
RNA	Ribonucleic acid
SDS	sodium dodecyl sulphate
TE	Tris-EDTA
TBE	Tris Borate EDTA
TEV	Tobacco Etch Virus
Tris	tris(hydroxymethyl)aminomethane
VHS	Video Home System
WT	wild type
YE	Yeast Extract
YE5S	Yeast Extract and 5 Supplements
3D	three dimensional

CHAPTER 1

Introduction

The Microtubule cytoskeleton and its structure

The microtubule (MT) cytoskeleton is important for many processes in the cell. MTs provide mechanical support for the cell to keep its shape, position the nucleus and organelles, serve as tracks for motor proteins to move cargos around the cell and are the most important structural element of cilia and flagella. During mitosis, they rearrange themselves into the mitotic spindle to push and pull chromosomes and finally segregate them into two identical sets before the cell divides (Fig.1.1). To perform all these functions, microtubules take advantage of their highly dynamic behaviour.

Figure deleted in the published version for copyright reasons.

Figure 1.1 MT cytoskeleton during the cell cycle.
Green: Microtubules. Blue: DNA. (mitchison.med.harvard.edu)

MTs are polymers constantly assembling and disassembling. They are built from alpha-beta tubulin heterodimer subunits, which initially assemble end-to-end into polar protofilaments (Amos & Klug, 1974). The protofilaments associate laterally to form a 25 nm wide tubular structure (see Fig. 1.2). MTs assembled in vitro have varying numbers of protofilaments, ranging from 10 to 16 with a majority of them having 14 protofilaments (Chrétien & Fuller, 2000). In vivo, the protofilament number is more tightly regulated and most MTs have 13 protofilament.

Figure deleted in the published version for copyright reasons.
See Akhmanova and Steinmetz, (2008) for the original drawing.

Figure 1.2. MT dynamic instability and structure.
a. Microtubules are composed of tubulin heterodimers that are aligned in a polar head-to-tail fashion to form protofilaments.
b. The cylindrical microtubule wall typically comprises 13 parallel protofilaments in vivo. The 3 subunit helical pitch generates a discontinuity in B lattice MTs called the seam (red dashed line).
c. Assembly and disassembly of microtubules is driven by the binding, hydrolysis and exchange of a GTP on the beta-tubulin monomer (GTP bound to alpha-tubulin is non-exchangeable and is never hydrolysed). Polymerization is typically initiated from a pool of GTP-Tubulin. Once tubulin is incorporated into the MT wall, its GTP is hydrolysed into GDP. The GDP-MT wall is metastable and can stochastically switch to a depolymerization state, realeasing GDP-Tubulin in solution. The cycle is completed by exchanging the GDP of the disassembly products with GTP, enabling the tubulin to start a new cycle. (Adapted from Akhmanova & Steinmetz, 2008)

There are two ways protofilaments can make contacts between each other. These two possible types of contacts define two different microtubule lattices. In the first one, the lateral contacts are between alpha and beta subunits, making a so-called A lattice. In the second one, the contacts are between alpha-alpha and beta-beta, making a B lattice (Fig. 1.3). A and B lattices were originally discovered by studying flagellar doublets. These doublets have one full MT, the A tubule and one partial MT, the B tubule,

clamping the first one. The A tubule was found to have a decoration of Microtubule Associated Proteins (MAPs) which corresponded to an A-lattice, whereas the B-tubule had a decoration pattern corresponding to a B lattice (Amos & Klug, 1974).

A B

Figure deleted in the published version for copyright reasons.
See Tilney et al., (1973) for the original pictures.

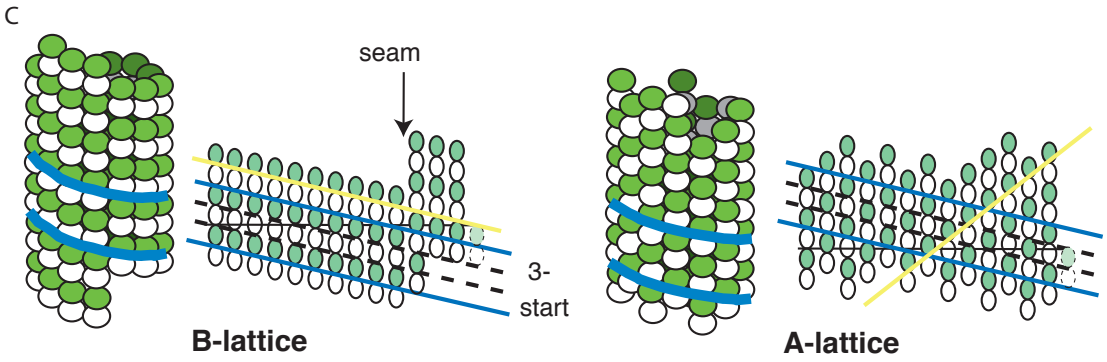

Figure 1.3. A and B lattices
A. Drawing of an outer doublet. The A tubule is composed of 13 subunits, the B of 11 subunits. **B.** Transverse section through the isolated flagellar axoneme of Lytechinus. 4% tannic acid. 330,000X. **C.** Diagrams of A and B lattices of MT subunits, represented both as 3D MTs and as opened-out sheets. White subunits, alpha-tubulin. Green subunits, beta-tubulin. Blue line, the direction of the 3-start family of helices, common to both lattices. Yellow lines, the direction of the decoration patterns, different on both lattices. (Panels A and B reproduced from Tilney et al. 1973)

The MT lattice of singlet cytoplasmic had not been studied when Song and Mandelkow looked at MTs assembled in vitro and decorated with kinesin heads, and discovered that they assembled mainly into a B surface lattice (Song & Mandelkow, 1993). Also, looking at flagellar doublets or MT extensions from flagellar doublets decorated with kinesin, they could only find B-lattice reflections (Song & Mandelkow, 1995). (This finding was not conclusive, as an inaccurate masking could have easily led to contribution of the B-tubule onto the A-tubule diffraction pattern. Also MT extensions were polymerised with Taxol, which has a strong effect on polymerisation.) The fact that MTs assembled in vitro always, or almost always displayed a B-lattice pattern

established the general belief that MTs only assembled with a B lattice (canonical lattice). However, the in vitro conditions used to polymerize tubulin are quite far from the cellular environment. For example, Dias and Milligan showed that MTs assembled with high salt conditions displayed a mixed lattice, with a higher proportion of A-lattice inter protofilament interactions (Dias & Milligan, 1999). MTs are polymorphous polymers that can assemble in various forms depending on the external factors applied to them. Glycerol or dimethylsulfoxide (DMSO) increases the protofilament number, high salt the proportion of A-lattice bonds, while zinc salts make tubulin assemble into sheets of antiparallel protofilaments. Therefore, the lattice actually used in the cell must be regarded as a totally open question; especially as, in vivo, many proteins must influence it. In particular, MTs never grow from any random place in the cell, but almost only from MT Organising Centres (MTOCs) such as Centrosomes (Fig. 1.4) (Stearns & Kirschner, 1994; Zheng, Wong, Alberts, & Mitchison, 1995). MTOCs nucleate MTs from gamma tubulin ring complexes (gamma-TuRCs)(Moritz, Zheng, Alberts, & Oegema, 1998) and it is very likely that the ring complex very rigidly defines the MT lattice. Therefore, in the light of present knowledge, the lattice of cellular microtubules cannot be taken for certain.

Figure 1.4. The centrosome.
A. The centrosome is the major MTOC of animal cells. Located in the cytoplasm next to the nucleus, it consists of an amorphous matrix of protein containing the gamma-tubulin ring complexes that nucleate microtubule growth. This matrix is organized by a pair of centrioles, as described in the text. **B.** A centrosome with attached microtubules. The minus end of each microtubule is embedded in the centrosome, having grown from a gamma-tubulin ring complex, whereas the plus end of each microtubule is free in the cytoplasm. (Adapted from Bruce Alberts et al. Molecular Biology of the cell. 2002.) **C.** Centrosome and nucleated MTs imaged by rotary shadowing on a carbon coated EM grid. Magnification: 5000x. (Mitchison & Kirschner, 1984.)

Principles of dynamic instability

MTs are able to deliver their cargo to any point in the cell thanks to their dynamic behaviour. They constantly switch from growth to shrinkage, which allows them to explore the whole volume of the cell. This dynamic instability is driven by the tubulin GTP-hydrolysis cycle (Mitchison & Kirschner, 1984). When GTP is bound to the tubulin beta subunit, tubulin is in a conformation allowing it to be incorporated into the microtubule. Once incorporated, the following tubulin alpha subunit provides a key catalytic residue and triggers GTP hydrolysis (Nogales, Wolf, & Downing, 1998). Tubulin is thought to undergo a conformational change upon GTP hydrolysis (or after the loss of Pi), putting strain in the MT lattice or/and loosening lateral contacts with the neighbouring protofilaments. The result of GTP hydrolysis is a more unstable MT, which can stochastically switch to rapid shrinkage, releasing GDP-tubulin in solution (Hyman et al., 1992; Ravelli et al., 2004). Once free in solution, tubulin can exchange its GDP for GTP and take part in assembly again (see Fig. 1.2).

During MT assembly, GTP hydrolysis is thought to happen with a certain lag. This lag has a consequence that if the MT is fast growing, the end of the microtubule must have a cap of GTP-tubulin. The GTP-cap model proposes that this stable cap of GTP subunits would provide the necessary stability for MT growth, preventing catastrophe events (Drechsel & Kirschner, 1994). Another model to explain MT dynamic behaviour is that growing ends have a specific structure. This structure would help stabilize MT ends and prevent catastrophes. Chrétien et al. observed that fast growing ends had a sheet-like extension that eventually grew wider before closing into a tube (see Fig. 1.5)(Chrétien, Fuller, & Karsenti, 1995). Such a structure is thought to be very stable. But MTs can also be seen growing with what appear to be blunt ends. The universal stabilizing end cap may therefore not be the sheet but may instead be a much less visible small difference in tubulin conformation or MT wall conformation (Janosi, Chrétien, & Flyvbjerg, 2002).

Figure deleted in the published version for copyright reasons.
See figure legends for reference to the original work.

Figure 1.5. Microtubule end structures.
MTs have different end structures whether they are fast or slow growing, pausing or shrinking. Cryoelectron microscopy of (a) depolymerizing and (b) polymerizing microtubule ends. (c) Diagrammatic representation of the structure of polymerizing (top) and depolymerizing (bottom) (images in (a) and (b) reprinted from Chretien et al 1995, (c) from Desai and Mitchison 1997).

Microtubule polarity and end structure: physiological importance

As tubulin assembles in a head-to-tail fashion, the MT has an intrinsic polarity. One end of the MT terminates with a crown of alpha subunits and is called the minus end, since it corresponds to the end that, in a cell, is almost always embedded in an MTOC in the centre of the cell; the other end has a crown of beta subunits and is called the +end. The +end is the most dynamic end in vitro, showing faster growth but also more frequent catastrophes than the minus end (Allen & Borisy, 1974). In vivo, of course, the +end is the only dynamic end and is a major interface in the search and capture mechanism (Mitchison & Kirschner, 1984). Its dynamic behaviour allows it to explore the volume of the cell and reach and connect to the cell cortex, chromosomes, or organelles. For example, in a motile cell, the MT +end will interact with the cell cortex of any protrusive zones and be stabilized at theses sites so that material can be transported into the protrusion (Mimori-Kiyosue & Tsukita, 2003). To regulate dynamics and attachment of MT +ends to cellular structures, there must be a complex machinery assembling specifically at this dynamic site. Thanks to technical advances in light microscopy, a family of proteins defined by their localisation at the plus end of growing MTs has

emerged. They are called +end Tracking proteins or +Tips (Schuyler & Pellman, 2001) and are very important for the regulation of the cytoskeleton morphology (see Fig. 1.6).

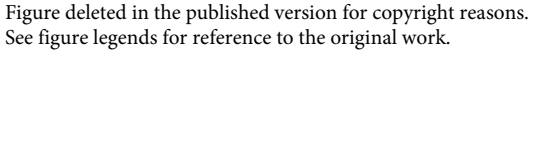

Fig. 1.6. The microtubule "search-and-capture" mechanism is governed by +TIPs.
a. The "search-and-capture" of microtubules. In an unpolarized cell (left), microtubules undergo assembly/disassembly behavior known as dynamic instability, in which microtubules coexist in growing and shrinking populations that inter-convert stochastically. The parameters of MT dynamic instability are defined as growth, shortening, the transition from growth to shortening (catastrophe), and the transition from shortening to growth (rescue). If a signal input activates some microtubule-capturing site at the cell cortex, MT stabilizing proteins such as +TIPs become more concentrated and stabilize MTs specifically at this site, which induces an asymmetric orientation of the microtubule-based cytoskeleton.
b. Localization of GFP-fused APC and EB1 in Xenopus A6 epithelial cells. GFP-APC clusters and stabilizes MTs at selected sites in the cell periphery, while EB1-GFP associates with every growing microtubule plus end throughout the cytoplasm.
c. The morphology of microtubules in budding and fission yeasts is governed by cortical sites, which also define growth zones. Adapted from Mimori-Kiyosue 2003.

3 classes of +end binding proteins:

Within the +Tips family of proteins, three classes can be defined: proteins that actively move to the MT end, proteins that bind specifically to the end and proteins that are brought there as cargo and accumulated by the two others (see Fig. 1.7)

The first class is mainly made up of proteins of the kinesin family of motor proteins. These kinesins can have different functions. They can be cargo transporters that use ATP to actively walk to the MT +end, efficiently accumulating other proteins at the end, such as the kinesin Kip2, actively bringing the Clip170 homologue Bik1 to MT ends, thereby enhancing its stabilization activity (Carvalho, Gupta, Hoyt, & Pellman, 2004).

Others, like the Kin1 family (MCAK), use the energy of ATP hydrolysis to destabilize the MT ends and trigger catastrophes (Moore et al., 2005; Desai, Verma, Mitchison, & Walczak, 1999). Some family members, such as *Drosophila* ncd, seem to be capable of both activities.

The second class of +Tips comprises proteins that bind specifically to the end of growing microtubules. Their mechanism of +end targeting is not well understood. There are two main model mechanisms for targeting the growing end of microtubules. The first one is recruitment of the protein by soluble tubulin and subsequent copolymerisation, followed by a release from the microtubule wall. The first +Tip to be discovered, Clip170 is thought to target MT ends in this way (Arnal, Heichette, Diamantopoulos, & Chrétien, 2004; Folker, Baker, & Goodson, 2005). It co-assembles with tubulin dimers or oligomers and is quickly released from the MT wall. Arnal et al. have observed that Clip170 interacts with free tubulin dimers and oligomers of high curvature, which then assemble into MTs. Clip170 and Clip170 family proteins are found to increase the frequency of MT rescue in vitro, therefore having a stabilization effect on MTs. At the same time they may serve as plus-end loading docks for other proteins such as the minus end-directed motor dynein and its associated cargo, or may dock on to kinetochores (Lansbergen et al., 2004).

Figure deleted in the published version for copyright reasons.
See figure legends for reference to the original work.

Figure 1.7 The 3 ways of Tip Tracking.
To accumulate at the growing MT +end, proteins can use three main ways: Binding specifically at the end by copolymerization or recognition of a specific structure at the MT end, by active transport (Kinesins), or as cargo of other proteins (Hitchhiking). (Adapted from Akhmanova & Steinmetz 2008)

The second possible mechanism of +end targeting is the recognition of and tight binding to a specific structure at MT ends, such as the sheet structure observed by Chrétien et al. (Fig. 1.5) or the GTP cap. The extent of the GTP cap is not known for certain, while its importance for microtubule stability and whether it has significant structural differences from the rest of the MT lattice are still unclear. MTs assembled with GMPCPP (a very poorly-hydrolysable analogue of GTP) are known to have a longer monomer repeat (42Å) compared to GDP MTs (40.5Å), suggesting that the tubulin dimers bound to unhydrolysed nucleotide must be in a more elongated or straighter form. However, the detailed structural difference between the two forms and whether it could affect MAP binding are not known. In contrast, the open flat sheets observed at the plus end of a growing MT, with its reverse curvature, is much more likely to provide very different binding sites from the closed MT wall, either on the flat lattice or on the edges of the open sheet, where tubulin dimers exhibit a face not normally accessible on the closed lattice. Recent papers hypothesise that the protein EB1 recognises this exposed structure and promotes tube closure by specifically stabilizing the seam of MTs (Sandblad et al., 2006; Bieling et al., 2007; Vitre et al., 2008). It was proposed to act as a molecular zipper, stabilizing the putatively weakest part of the MT wall. Although EB family proteins have been widely seen as MT stabilizers, mainly suppressing catastrophes, the molecular mechanism of such effect is still completely unknown.

Another type of +end-targeted proteins can be found in the XMAP215 family. These proteins seem to target the MT +ends irrespective of their dynamic state. They have been found to interact with taxol stabilized MTs and to be MT destabilizers in some cases (Spittle, Charrasse, Larroque, & Cassimeris, 2000; Kinoshita, Arnal, Desai, Drechsel, & Hyman, 2001; Slep & Vale, 2007; Popov & Karsenti, 2003). They must be recognising a different feature of the MT end from the EB1 family to explain such difference in behaviour.

The third class of +Tips are proteins that may or may not bind directly to MTs but are targeted to the +end by interacting with the two other classes (hitchhiking). They can have very diverse functions, including serving as molecular adaptors to other cellular structures, such as cortical actin or kinetochores, or acting as signal transduction molecules, such as APC, which needs to be brought to specific places in the cell (Lansbergen & Akhmanova, 2006). An important example in *S. pombe* is the cell end marker Tea1, (Mata & Nurse, 1997; Behrens & Nurse, 2002). Minus end motors such as the dynein/dynactin complex are taken to plus ends where they can then exert force on cellular structures by pulling towards the minus end or actually take cargoes back to the centre of the cell (Vaughan, Miura, Henderson, Byrne, & Vaughan, 2002). Some of these proteins, like APC, can bind to MTs by themselves but are concentrated at the tip by +end tracking proteins, EB1 in this case (Akhmanova & Hoogenraad, 2005).

A tip-tracking complex required for S. pombe cell polarity maintenance

In the fission yeast *S. pombe*, a tip-tracking complex that seems to comprise most of these classes of proteins has been identified. It includes the kinesin-like protein Tea2 (see Fig.1.8), the Clip170 homologue Tip1 and the EB1 homologue Mal3. Deletion of any of these 3 proteins gives rise to very similar phenotypes: MTs are shorter and fail to deliver cell end markers, such as Tea1, to the tip of this rod-shaped cell. The result is that the cell loses its well-defined polarity and becomes bent or branched, being unable to define its growth directionality (see Fig. 1.9)(Beinhauer, Hagan, Hegemann, & Fleig, 1997; Browning et al., 2000; Brunner & Nurse, 2000; Behrens & Nurse, 2002; Browning, Hackney, & Nurse, 2003; Busch, Hayles, Nurse, & Brunner, 2004). The phenotype similarity and the fact that the three proteins interact with each other make it a very well defined complex where all proteins seem to work in concert. But it is not known how each of these components affect MT stability by itself or which role each protein plays in this complex.

Figure deleted in the published version for copyright reasons.
See figure legends for reference to the original work.

Figure 1.8. Localization of Tea2p in logarithmic phase cells.
Tea2 viewed in fixed cells. (A, B) tea2-GFP cells fixed and stained with antibodies to GFP (Green), tubulin (red). (C, D) Wild-type cells fixed and stained with antibodies to Tea2p (green), tubulin (red), DNA stained with DAPI (blue) Bar: 5 μm. Adapted from Browning et al. 2000.

Tea2 is a +end directed kinesin-like protein and so has the likely function to increase the local concentration of the two other components at the +end (Busch et al., 2004). Tip1 is a close homologue of Clip170 but lacks one of the two MT-binding CAP-Gly domains of Clip170 (Brunner & Nurse, 2000). The human Clip170 has been shown to be a microtubule stabilizer but the difference in domain organisation of the two proteins might give them a different function. Tip1 binds to Tea2 via their extensive coiled coil domains (Busch et al., 2004), which also serves as binding domain for other cargos, such as the cell end marker Tea1 (Brunner & Nurse, 2000). Mal3 binds to Tea2 kinesin head domain and Tip1 CAP-Gly domain via its coiled-coil EB1 domain (Browning & Hackney, 2005).

Tea2 and Tip1 always colocalise inside the cell but Mal3 is not exclusively restricted to this complex (Browning et al., 2003; Busch et al., 2004). It can be seen in other locations, such as on the MTOC and seems to bind more transiently to the complex than its two partners. For example, when a MT is captured by the cell cortex, Tea2 and Tip1 stay attached to this site, whereas Mal3 quickly vanishes before the MT undergoes catastrophe (Busch & Brunner, 2004).

Figure deleted in the published version for copyright reasons.
See figure legends for reference to the original work.

Figure 1.9. Influence of Tip1 on Microtubules and cell end marker Tea1 localization
(A–D) Calcofluor staining of wild-type and Δ-tip1 cells to show the directionality of growth.
(A) Wild-type cells grow in a straight line. **(B)** Exponentially growing Δ-tip1 cells are bent (~80%) and at low frequency branched (~1%). **(C)** Δ-tip1 cells 2 hr after recovery from nutritional starvation. Seventy to eighty percent of the cells are branched. **(D)** Δ-tip1 cells 2 hr after recovery from nitrogen starvation. Seventy to eighty percent of the cells initiate growth at an oblique angle to the longitudinal cell axis at one or both cell ends.
(E, F) Immunofluorescence of wild-type and Δ-tip1 cells with anti-tea1p (green) and/or anti-tubulin (red) antibodies.
(E) In wild-type cells the majority of the microtubules span the entire length of the cell, and they are aligned parallel to the long axis of the cell. Tea1p accumulates at the cell ends and is also found on microtubules. **(F)** In Δ-tip1 cells, microtubules are less oriented and short, reaching on average only 30%–60% of the length of wild-type microtubules. Tea1p is localized along microtubules, but only little tea1p is present at the cell ends. (Adapted from Brunner & Nurse 2000.)

Although it seems clear that the main functions of this tip tracking complex are to stabilize the axial MT array and to deliver cargoes to the cell tip, the precise functional relationship between the three proteins is unknown and mainly restricted to in vivo studies. Therefore, the aim of this work was to reconstitute an in vitro system that could provide clues about the precise function of each of these three proteins and their relation with the others.

For that aim, two strategies were used:

The first strategy was to extract the endogenous complex with a protein A tag fused to them. This method has the advantage to eventually recover the fully working endogenous complex in its native state and additional unknown proteins that could be part of it.

The second strategy was to clone, express and purify recombinant proteins separately in *E. coli* and reconstitute the complex in vitro, in the hope that it would be fully functional, to be studied by biochemical and structural methods.

CHAPTER 2

Isolating a +Tip tracking complex by protein A pull-down in *S. pombe*

Strategy

The protein A (prA) from *S. aureus* binds IgG antibodies with very high affinity. It has been successfully used in the past to affinity-purify tagged proteins expressed in bacteria with IgG sepharose chromatography (Moks et al., 1987). It has also been used in yeast to purify prA-tagged calmodulin (Stirling, Petrie, Pulford, Paterson, & Stark, 1992) and to identify proteins in high molecular weight complexes in yeast (Grandi, Doye, & Hurt, 1993; Knop & Schiebel, 1997; Wigge & Kilmartin, 2001).

By tagging one known protein of a complex with the prA sequence directly onto the gene, that protein can be expressed with the prA tag at the endogenous level. This avoids the risk of disrupting the complex or the complex function because of an incorrect level of expression of one of its components. Thereby, this complex can be affinity-purified with more chance to recover it in its fully functional state. This can allow biochemical or structural studies if the complex is recovered in large enough quantities or analysis of its constituents' identities and stoichiometries with the help of MALDI peptide analysis (Wigge et al., 1998). As the prA tag binds with very high affinity to IgG antibodies, the complex can be purified very quickly, lowering the chances for the complex to fall apart or lose constituents, and with very little contaminants, making the mass spectrometry analysis accurate.

It is important to have different proteins tagged and if possible at different locations on each protein as there is a chance that the tag will interfere with the complex formation

or function.

To apply this strategy to the *S.pombe* +Tip complex, its 3 characterised components, Mal3, Tip1 and Tea2 were tagged individually with three prA IgG binding domains at their C-terminal (Fig. 2.1) and the experiments were performed with each of them.

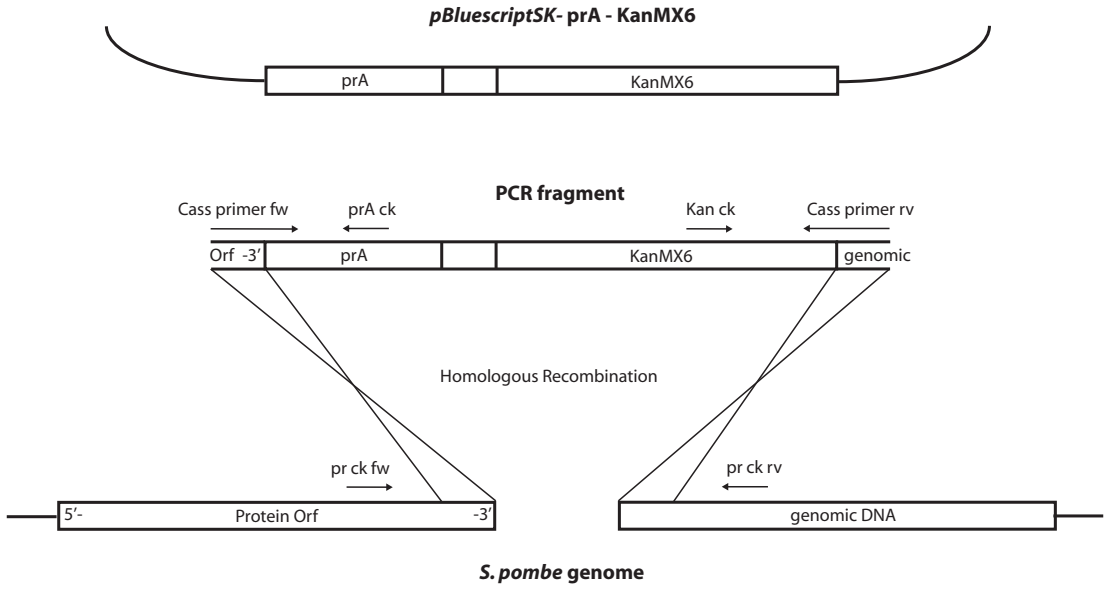

Figure 2.1 protein A insertion by homologous recombination.
The DNA cassette is amplified from a bluescript SK- vector containing the protein A repeats followed by the KanMX6 cassette. **Arrows** show primers position. Forward primers (Cass primer fw) contain the orf's 50 last 3'end nucleotides followed by the 20 first nucleotides of the cassette. Reverse primers (Cass primer rv) contain the 20 last nucleotides of the cassette followed by the 50 nucleotides that are after the orf's stop codon.
Three protein A repeats are inserted at the orf 3' end just before the stop codon. It is followed by a KanMX6 cassette giving resistance to Geneticin. **Arrows** show the position of primers used to check if homologous recombination has occurred at the right place (ck primers).

Table 2.1 Pull Down Primers

	5' 3'
Tip1 cass fw	ATCATTCATTGCAGGAATGTCCCACTGTATTTGGCAGCACAGACGAAGCT GGTGAAGCTCAAAAACTTAAT
Tip1 cass rv	CATGCTGAAGATACAGCTATTACATTATGACCAGAAGTGGTCATATATAT CTCGAGGTCGACGGATCCCC
Tip1 ck fw	GCGGAGAAAGAAAATCTTGTATCA
Tip1 ck rv	TTAAAAATTAAATACGTTTTA
Mal3 cass fw	ATGCTAGGCTACAAAGTTTAGAGGTTGATGACGATGAGAATATCACGTTTGGTGAAGCTCAAAAACTTAAT
Mal3 cass rv	AGTGAAAAATGAAGAATTTGCAACAAAAAAAAACTTTAACTTAGTACTTT CTCGAGGTCGACGGATCCCC
Mal3 ck fw	ATGTTGGAGCGTATTCAAGCA
Mal3 ck rv	AAGGATTAAAGTTTATTACAA
Tea2 cass fw	AACAGCAATCGAAAAAGGATTCTGTGACTCAGGAAACGCAACTTCTTTCT GGTGAAGCTCAAAAACTTAAT
Tea2 cass rv	TAAAATTGTAAACAAGGTTGATGAGAAGACGCCTATAATTAAACAAGGTA CTCGAGGTCGACGGATCCCC
Tea2 ck fw	AAGATAAAGAACAAATTATTT
Tea2 ck rv	AAATTTTGCATAGAGAAGCCA
Kan ck	GCTAGGATACAGTTCTCACATCACATCCG
prA ck	AACAAAGAACAACAAAATGCTTTCTATGAA

Methods

Schizosaccharomyces pombe strains

S. pombe strains were constructed by recombinant PCR: transformation with a PCR fragment followed by homologous recombination (Bahler et al., 1998), in a wild type strain IH365 h^- (Bridge, Morphew, Bartlett, & Hagan, 1998). Backcrossings were done with the strain IH366 h^+.

PCR amplification of the protein A cassette

PCR primers were 70 nucleotides long (see Table 2.1); they were synthesized and PAGE purified by Sigma. DNA fragments were amplified using the KOD Hot start DNA Polymerase (Novagen) and the plasmid shown in Figure 2.1 as template. PCR reactions were performed in 200 µl PCR tubes. The PCR mix (total volume, 600 µl) contained 60 µl of KOD buffer with 1 mM $MgSO_4$, 1 mM of each dNTP, and 0.5 µM of each primer, 3 M Betaine, 1 µg of DNA template, and 24 µl of KOD enzyme mixture. 35 cycles of 95°C for 1 min, 55°C for 30 sec, and 72°C for 8 min were executed (see Fig 2.2). The products from 12 PCR reactions (10–20 µg of DNA) were pooled, precipitated with ethanol, and resuspended in 15 µl of water. This concentrated DNA was used directly for transformation of S. pombe cells.

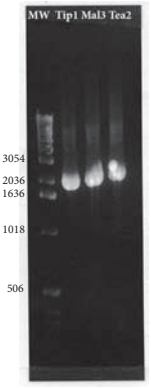

Figure 2.2. Cassette PCR poly-acrylamide gel electrophoresis of the cassette PCR products.

Transformation of S. pombe and selection of G418-resistant clones

S. pombe cells were transformed with the PCR fragments using a protocol based on the method of Keeney and Boeke (Keeney & Boeke, 1994). Wild-type cells were grown at 30°C in YE medium with 5 supplements (YE5S, adenine, histidine, leucine, uracil

and lysine at 225 mg/l) (Moreno, Klar, & Nurse, 1991) to about 10^7 cells/ml (50 ml/transformation). Cells were washed once with an equal volume of water, and the cell pellet was resuspended in 1 ml of water, transferred to an Eppendorf tube, and washed once with 1 ml of LiOAc/TE made from 10X filter-sterilized stocks (10 x LiOAc: 1 M lithium acetate, adjusted to pH 7·5 with diluted acetic acid; 10 x TE: 0.1 M Tris–HCl, 0.01 M EDTA, pH 7.5). The cell pellet was then resuspended in LiOAc/TE at 2 x 10^9 cells/ml. 100 µl of the concentrated cells were mixed with 2 µl sheared salmon sperm DNA (10 mg/ml) and 10 µl of the transforming DNA. After 10 min incubation at room temperature, 260 µl of 40% PEG/LiOAc/TE (for 20 ml of solution: 8 g of PEG 4000 dissolved in 2 ml of 10 x LiOAc, 2 ml of 10 x TE, and 9.75 ml water, and filter sterilized; can be stored up to 1 month) was added. The cell suspension was mixed gently and incubated for 30–60 min at 30°C. 43 µl of DMSO were added, and the cells were heat shocked for 5 min at 42°C. Cells transformed with fragments carrying the kanMX6 marker were then washed once with 1 ml of water, resuspended in 0.5 ml of water, and plated onto two YE plates (250 µl/plate). These plates were incubated for 18 hrs at 30°C, resulting in a lawn of cells. The cells were then replica plated onto YE plates containing 100 mg/l G418/Geneticin (GIBCO; G418 was added after autoclaving the medium, and plates were stored at 4°C). The replica plates were incubated for 2–3 days at 30°C, and large colonies were restreaked onto fresh YE plates containing G418. (The tiny colonies appearing on the initial G418 plates were not stable transformants.)

Screening transformants for homologous integration by PCR

G418-resistant clones were checked by PCR for integration of the DNA fragment by homologous recombination. A lump of cells was heated at 95°C in 0.25% SDS for 5 min and spun down. 1µl of the supernatant was then used as template for a PCR reaction using KOD Hot Start DNA Polymerase. Primers were designed to amplify fragments of

known size across junctions between the genomic DNA and the inserted fragment and across the whole fragment (see Table 2.1 and Fig. 2.1). PCR products of the expected size should be observed if the DNA had integrated by homologous recombination at the targeted gene (Fig. 2.3).

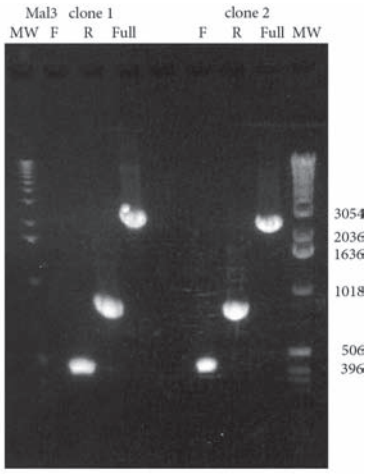

Figure 2.3 Colony PCR check
Two clones with prA inserts at Mal3 C-terminus were checked by PCR for correct position of the insert. F checks the junction between Mal3 3' end and prA sequence with primers Mal3 ck fw and prA ck. R checks the junction between the KanMX6 and the genomic DNA following Mal3 ORF with primers Kan ck and Mal3 ck rv (See Figure 2.1 and Table 2.1). Full is the amplification of the whole insert with primers Mal3 ck fw and Mal3 ck rv. Expected length: F: 415 nucleotides, R: 859, Full: 2389. Tea2-prA and Tip1-prA clones gave similar results.

Backcrossing

To determine if the transforming fragment had integrated at a single site in the genome, strains with a positive PCR reaction were crossed against a wild-type strain, tetrads were dissected, and the resulting spore colonies were analyzed for a 2:2 segregation of G418 resistance (together with the correlated positive PCR reaction).

For this, h- and h+ strains were streaked out on YE5S plates for freshly growing cells the next day. The strains were mixed on a mating plate (MEXS, 3% malt extract (Difco) adjusted to pH 5.5 with NaOH, 2% agar (Difco) or MSL-R, 10 g glucose, 1g KH_2PO_4, 0.1 g NaCl, 0.2 g $MgSO_4 \cdot 7H_20$, 0.1 g $CaCl_2 \cdot 2H_2O$, 0,1 g minerals, 2 ml vitamins, 25 g agar/l) with sterile sticks and a little sterile water. They were left at 29°C to mate and sporulate. U-shaped asci with 4 clear spores in them were checked in the phase contrast microscope at 2 days.

The cells were then streaked out of the mating plate with a toothpick down the side of

a YE5S plate to get a steadily decreasing number of cells down the streak. Asci were selected and picked in a Singer machine and incubated at 37°C for 4 to 8 hrs. Plates were checked after 4 hrs, looking for a change in shape suggesting that the asci had started to germinate. When germination had started, spores were quickly picked before they could mate again. The spore colonies were then streaked on a plate and resistance to G418 tested on a replica plate. Freshly growing cells were then again mixed with the mating tester strain and asci looked for after 2 days.

h+ and h- G418 resistant strains having correctly segregated were stored in 15% glycerol at -80°C.

Western blotting

To check for expression of Tip1-prA, Mal3-prA and Tea2-prA in yeast, total cell lysates were analysed by SDS-PAGE and Western blotting; the blot was directly probed with IgG coupled to horseradish peroxidase, which specifically binds to the protein A moiety of the fusion protein. In a control WT strain, no cross-reaction with endogenous yeast proteins was seen. In the Tea2-prA and Tip1-prA expressing strain, bands around 78 kDa (which is the expected size for the fusion protein) were visible (Fig. 2.4). The first Mal3 clones did not express the tagged protein but new transformants obtained later did (Fig. 2.4 right).

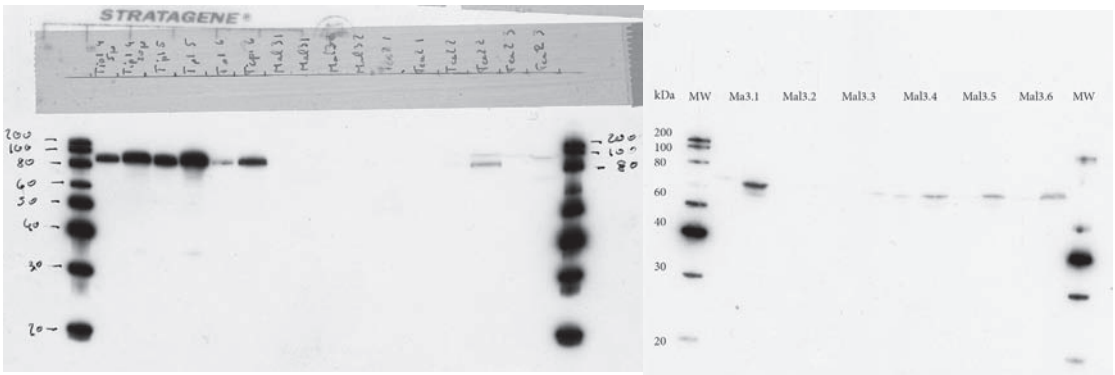

Figure 2.4 Colony Western blot
(Left) Cells were lysed in SDS, spun down and the supernatant loaded directly onto the gel. 5 and 20 µl of each clone was loaded side by side. prA tagged proteins of the expected size were found for all Tip1 clones and Tea2 clone 2. No protein with a prA tag was found for the Mal3 clones.
(Right) Mal3 clones were lysed in SDS, spun down and the supernatant loaded directly onto the gel. 5 and 20 µl of each clone

was loaded side by side. prA tagged proteins of the expected side were found for Mal3 clones 1, 4, 5 and 6. Clone 1 seems to have better expression levels.

Purification of the +Tip Complex for Mass spectrometry analysis

One liter of cells harvested at 4 x 10^7 cells/ml was rinsed with PBS and lysed with a cryo grinder (2 g of cells). Lysis was checked under the phase contrast microscope. The fine powder was then thawed in 8 ml of NP40 buffer (6 mM $NaHPO_4 \cdot H_2O$, 1% Nonidet P-40, 150 mM NaCl, 50 mM NaF, 20 mM glycerol phosphate, 4µg leupeptin), with 1 complete EDTA free tablet (Boehringer Mannheim) and 500µl 0.1 M PMSF in 100% ethanol. After centrifugation at 45 krpm in a Ti45 rotor, 20 µl IgG-Sepharose beads (Amersham Pharmacia Biotech) were added to the lysate and incubated for 1 hour. The lysate and the beads were then passed through a Biorad Poly-prep chromatography column by gravity and the beads washed with 30 ml IPP 150 buffer (10 mM Tris-Cl, pH 8, 0.150 M NaCl). Beads were then washed with 3ml NH_4Ac pH 5.5 and eluted with 100 µl 0.5 M acetic acid pH 3.4. Fractions were concentrated by freeze-drying and resuspended in 25 µl loading buffer. They were boiled 3 min. 20 µl was loaded on a first gel and 5 µl on another for western blotting (see Fig. 2.5).

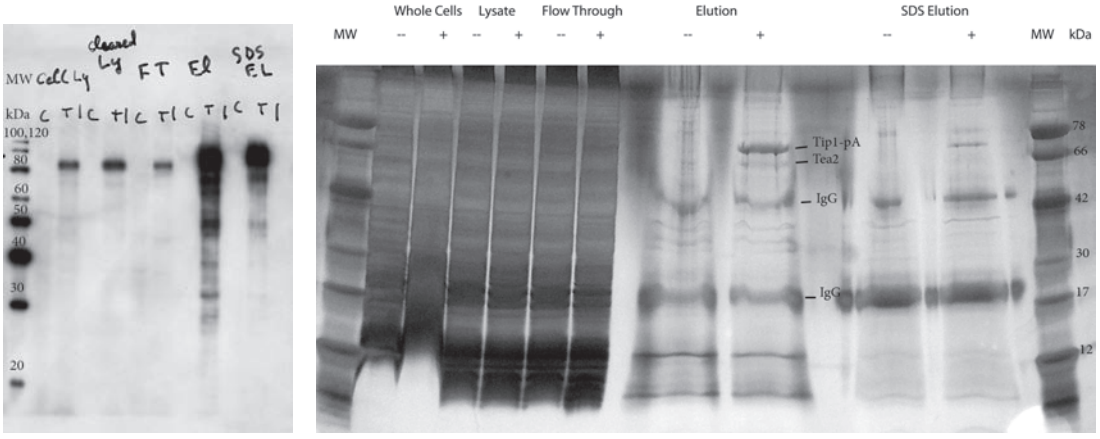

Figure 2.5 Tip1-prA Pull Down.
(Left) Western Blot C: Control experiment with WT cells. T: Experiment with Tip1-prA cells. Cell ly: cell lysate, Cleared ly: cleared lysate, FT: flow through. El: elution with 100 µl Acetic Acid pH3.4, SDS EL: elution with SDS to check what remained bound to the column. **(Right) pull down SDS-Page.** Lanes with the sign – are from the control experiment with WT cells. Lanes with the sign + are from the experiment with Tip1-prA cells. The sample is eluted with 100 µl Acetic Acid pH3.4 followed by an elution with SDS. The two top bands are the only bands clearly different from the control experiment. They are identified as Tip1-pA and Tea2 by mass spectrometry.

Mass Spectrometry

Proteins in SDS gel bands were identified by mass spectrometry. Gel bands were digested with trypsin (Wigge et al., 1998) and the tryptic peptide masses were determined by MALDI mass spectrometry in a PerSeptive Biosystems Voyager-DE STR mass spectrometer using external standards or matrix peaks and trypsin peptides as internal standards. The National Center for Biotechnology Information non- redundant database of about half a million proteins was searched using MS-fit (available at http://prospector.ucsf.edu) set at 50 parts per million, 0–300 kD. The proteins identified were the top match with MOWSE (Pappin, Hojrup, & Bleasby, 1993) scores (P factor 0.4) of between 3 x 10^5 and 4 x 10^{17}. A second search allowing methionine oxidation, protein NH2-terminal acetylation, and two missed tryptic cleavages was then carried out to match further peptides.

Results

Mass spectrometry analysis

The protein A pull down confirmed Tip1 and Tea2 interaction (see Figs 2.5 and 2.6). It suggests that they form a tight complex. As they are always seen in similar proportions on all the experiments performed they probably form a 1 to 1 complex. Surprisingly, Mal3, which is also a known interactor, could never be found in these experiments. Mal3 must have a much more labile interaction with Tip1 and Tea2 and therefore may not be retained. This supports the observation by FRAP that Mal3 has a much faster turnover than Tea2 and Tip1 at growing MT tips (Busch et al., 2004). No other binding partners could be identified with absolute certainty. It means that there are no other tight interactors in this complex. Most proteins that bind to this complex must be cargo proteins and therefore may have a labile interaction with their carrier.

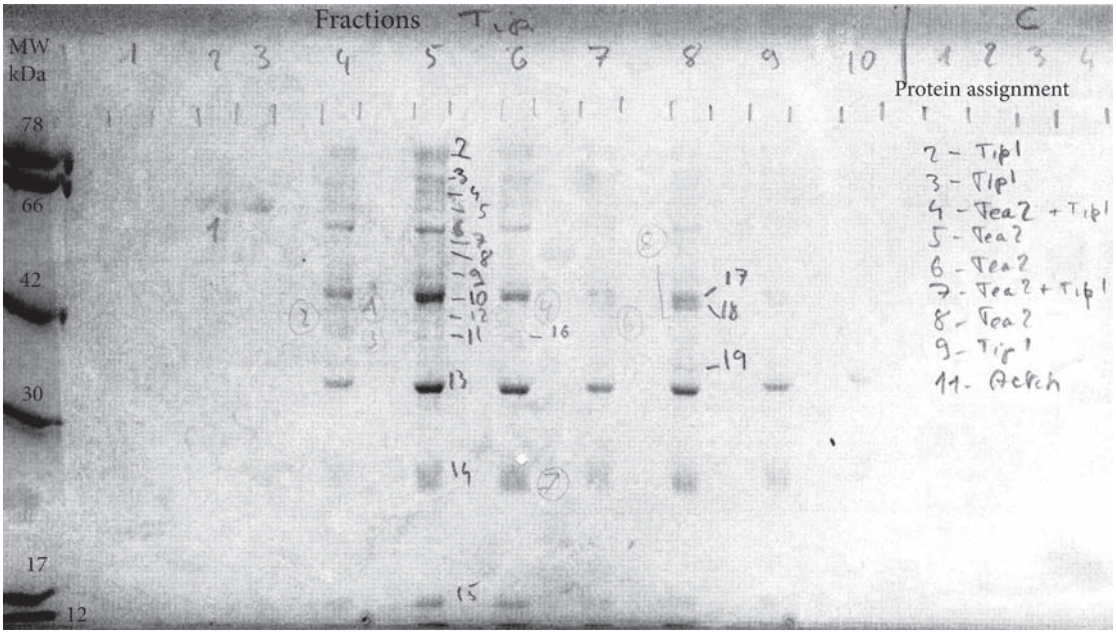

Figure 2.6 Tip1 pull down fractions
The gel is loaded with samples separated by one lane. The first 3 lanes are fractions from the NH4Ac pH 5.5 wash. The sample is then eluted with 100 µl Acetic Acid pH3.4 (lines 4-10). Left: Mass spectrometry protein assignment of the isolated bands. Are shown only the MOWSE top matches. Numbers which don't have an assignment are non analysed bands or containing IgG light and heavy chains. Many bands of this experiment are the result of proteolytic cleavage of Tip1 and Tea2 proteins. Actin is a possible interactor but is also often found as contaminant in pull downs.

Affinity purification of Tea2-prA, Tip1-prA by IgG-Sepharose chromatography

Since prA fusion proteins appeared to be expressed properly in the *S. pombe* cell, an attempt was made to purify the protein complex under non-denaturing conditions. As the proteins were expressed at their endogenous level, and as they are in relatively low number in these cells, maybe a few hundreds per cell at most, an attempt was made to grow the cells as 100 l fermentor batches and scale up the purification process to circumvent that problem. Lower yield of binding to the IgG and protein degradation due to the slower purification process complicated the task. This technique appeared not to be the most convenient to purify this particular complex. Also, the finding that only Tip1 and Tea2 associated tightly, with no other major components involved, made the bacterial expression of each protein individually much more appealing. Reconstituting the complex in vitro should be feasible and its biochemical characterisation eased by the much higher yield of expression of this system.

CHAPTER 3

Expression and purification of Mal3, Tip1 and Tea2 from *E. coli.*

Strategy

Protein sequences were analysed using NCBI Blast, the MacStripe Lupas algorithm for coiled coil prediction (Lupas, Van Dyke, & Stock, 1991), the Sanger Pfam database and experimental data from the literature (Busch et al., 2004; Honnappa, John, Kostrewa, Winkler, & Steinmetz, 2005). Known or putative protein domains were defined and were cloned for expression in bacteria using a plasmid vector. Constructs of interest included:

Mal3 full length, Mal3 putative MT binding domain alone and putative MT binding domain followed by the low complexity region linking it to the coiled coil dimerisation domain (Honnappa et al., 2005).

Tip1 full length, Tip1 putative MT binding domain alone, Tip1 putative MT binding domain followed by the low complexity region linking it to the coiled coil dimerisation domain and Tip1 MT binding domain with a small part of the dimerisation domain.

Tea2 was expressed and purified following Browning & Hackney (2005) by Miho Katsuki at the Marie Curie Research Institute (MCRI), Oxted.

Biochemical and structural characterization of these constructs interaction with microtubules were done with tubulin purified both from pig brain and from *S. pombe*. *S. pombe* tubulin was purified by Michael Osei at MCRI, Oxted.

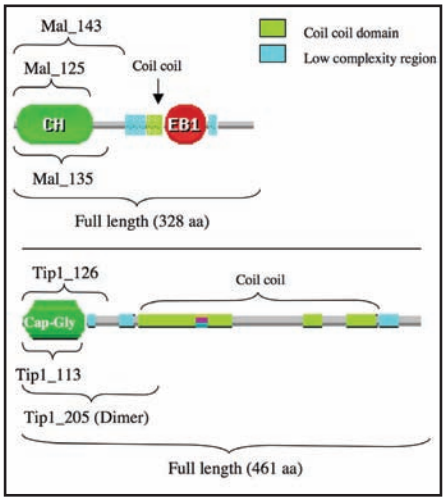

Figure 3.1 Tip1 and Mal3 constructs. Constructs as shown by brackets on this Pfam domain organization graphic were designed, expressed in *e. coli* and purified. (Adapted from http://pfam.sanger.ac.uk)

Methods

Preparation of a S. pombe cDNA library

The presence of an intron in the Mal3 gene complicated the direct cloning by PCR amplification of the genomic DNA. To circumvent that problem an *S. pombe* cDNA library was built and the gene constructs PCR amplified from it.

S. pombe cells were grown to log phase and lysed to extract their total RNA with a Qiagen RNeasy mini kit. Poly(A)+ mRNAs were purified from total RNA using the Oligotex mRNA kit (Qiagen). Reverse transcription of the Poly(A)+ mRNA was made with StrataScript reverse transcriptase (Stratagene) and oligo(dT) primers. cDNA synthesis was achieved according to the supplier's instructions (Stratagene).

Oligonucleotide synthesis

Oligonucleotides were either synthesized in-house (MRC oligonucleotide synthesis service) or purchased from Sigma, U.K. or Operon Biotechnologies GmbH. (See Table 3.1)

Table 3.1 PCR Primers

Tip1fwnde1 for pHis17	5' atactagcatatgtttcctcttggcagtgtc 3'
Tip1rvBam113 for pHis17	5' taactacggatccaacattggttaatcttggaat 3'
Tip1rvBam126 for pHis17	5' tagctacggatccaatagtattcatactgagatt 3'
Tip1rvBam205 for pHis17	5' tatatacggatcctctccgttgtgaagcctcatt 3'
Tip1rvBam461 for pHis17	5' tatatacggatccagcttcgtctgtgctgccaaa 3'
Tip1fwbamh1 for pGEX-4T-1	5' atactagggatccatgtttcctcttggcagtgtc 3'
Tip1rvXho461 for pGEX-4T-1	5' tagctacctcgagttaagcttcgtctgtgctgccaaa 3'
Mal3fwnde1 for pHis17	5' atactagcatatgtctgaatctcggcaagagctc 3'
Mal3rvbam105 for pHis17	5' tagctacggatccatattgatcccaaaaacgttt 3'
Mal3rvbam123 for pHis17	5' tagctacggatccagcaggtcctctattcccccg 3'
Mal3rvbam135 for pHis17	5' tagctacggatccagttgctcctgcagaggaatt 3'
Mal3rvbam143 for pHis17	5' tagctacggatccaacctgacggcgacgagaagg 3'
Mal3rvbam328 for pHis17	5' tagctacggatccaaacgtgatattctcatcgtc 3'

Gene amplification by polymerase chain reaction (PCR)

Genes and fragments of genes of interest were amplified using PCR. 50 µl reactions consisted of: primers to a concentration of 0.2 to 0.5 µM; 20 to 200 ng of template DNA, depending on the quality of DNA, 0.2 mM dATP, dTTP, dCTP, dGTP and 1 mM magnesium sulphate; 1x KOD polymerase reaction buffer and 2.5 units of KOD Hot Start DNA polymerase (Novagen, UK). PCR cycle: initial 2 min hot start at 95°C (melting), 30 sec at 60 ± 10°C gradient (primer annealing), 30 bp/s extension time at 72°C, 30 sec at 95°C (melting). The latter three steps were cycled 35 times. Five to twelve reactions would be set up across the gradient (see Fig. 3.2).

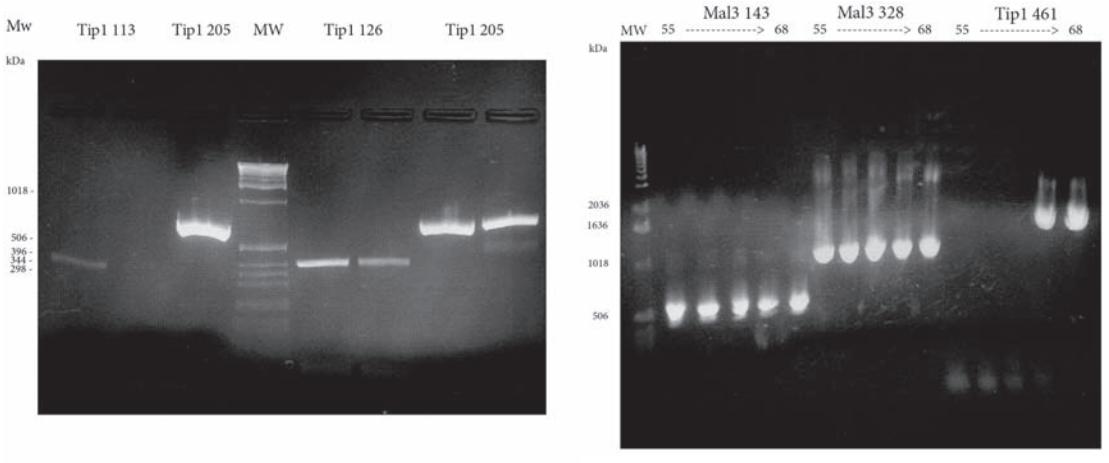

Figure 3.2. Agarose gel electrophoresis of PCR products.
Left: Tip1 PCR fragments. Each PCR performed with 2 different cDNA libraries: retrotranscription with poly-A primers (left lanes) and with random primers (right lanes). the cDNA library generated with poly A primers gave more consistent results and was used in all subsequent PCR reactions.
Right: Mal3 and Tip1 full length PCR fragments. An anealing temperature gradient (55 to 68°C, left to right) was performed. Tip1 full length fragment was only amplified with anealing temp. between 65 and 68 °C.

PCR purification

PCR reactions were purified using a QIAquick PCR Purification Kit (Qiagen, UK) and were eluted in 30 µl 10 mM Tris-Cl pH 8.0.

DNA restriction endonuclease digest

Restriction endonucleases from New England Biolabs were used according to the supplier's instructions to cleave PCR products and plasmid DNA, and to generate sticky ends. For cloning, digests were typically 3 hrs long at 37°C. Digests were stopped and purified with the QIAquick PCR Purification Kit to remove the small cleaved fragments.

Vector preparation

Plasmid DNA (pHis17, pOPTG or pGEX-4T1) was linearised by the desired restriction digest for 3 hrs at 37°C. Calf alkaline phosphatase (Roche, UK) was added directly to the digest with, typically, 20 units per 30 µl of DNA sample for 30 mins at 37°C. Alkaline phosphatase removes 5' phosphates from plasmid vectors that have been cut with a restriction endonuclease. This treatment prevents self-ligation of the vector in subsequent ligation reactions, and thereby facilitates ligation of other DNA fragments into the vector. To remove unwanted insert cleaved from the vector, the desired digest product was separated from the contaminant by size using agarose gel electrophoresis, excised and extracted from the gel.

Agarose gel electrophoresis

For the separation of DNA by size, melted 1 % to 2% agarose in 0.5x TBE (Appendix) mixed with 0.5 µg/ml ethidium bromide was poured into a gel casting tray and

electrophoresis apparatus and left to solidify at room temperature. DNA was loaded with agarose gel loading buffer (Appendix) and the gels run in 0.5x TBE buffer at 90 V for 45 min. Gels were visualised with a UV transilluminator and photographed. A molecular weight standard derived from a digested 1 kilobase DNA plasmid was run as a reference band (Life Technologies, Gibco BRL, UK).

DNA gel extraction

PCR reactions contaminated with undesired DNA products or linearised vectors were gel purified using a QIAquick Gel Extraction Kit and eluted in a final volume of 30 µl 10 mM Tris-Cl pH 8.0.

DNA insertion and ligation

Typically, 7 µl suitably digested purified linear DNA insert was mixed with 1 µl vector preparation, 1 µl 10x T4 DNA ligase reaction buffer and 1 µl T4 DNA ligase (400 units/ µl) (New England Biolabs). The reaction was left for 2 hrs at room temperature before transformation.

E.coli transformation into cloning strains

Prior to transformation, either *E.coli* TG1tr or DH5-alpha electrocompetent cells were thawed and left on ice. 5 µl of ligation reaction was added to 100 µl *E.coli* and left to mix for 10 mins on ice in a 2 mm electroporation cuvette. Cells were transformed at 2.5 KeV, 25 µF capacitance and 100 Ohms resistance. 250 µl 2x TY growth medium was immediately added to the electroporation cuvette. The mix was then spread onto TYE agar plates containing the appropriate selective antibiotics and left at 37 °C overnight.

Plasmid amplification and purification

1 to 100 colonies were typically recovered on each plate. In general, 3 clones were picked and grown overnight in 5 ml TY medium with antibiotics. 4 ml of culture were harvested and the plasmid purified using the Qiagen miniprep kit. The remaining mililitre was mixed with 30% glycerol, flash-frozen in liquid nitrogen and stored at -80°C.

DNA sequencing

Purified plasmids were sent to MRC-Geneservice (UK) for their insert to be sequenced. T7 or pGEX forward and reverse priming sites were used.

Culturing of E. coli clones

When plasmids with the correct insert were obtained and their sequence verified, 1 µl of the plasmid DNA of interest (~ 100 ng/µl) was added to 50 µl aliquots of the desired protein expression strain, and was treated and transformed as above and grown overnight on TYE agar plates containing the appropriate selective antibiotics. One colony was then picked the next evening to start a 120 ml culture to be grown overnight. It is important to respect this schedule, as an older colony, left too long in stationary phase, would not yield the same level of protein expression.

Expression of His-tagged protein constructs

E.coli C41 or Bl21 strains transformed with the vector for Mal3-His6 (plasmid pHis17-Mal3) or Tip1-His6 (pHis17-Tip1) were grown in 120 ml 2x TY supplemented with 100 µg/ml ampicillin at 37°C overnight, and shaken at 200 rpm. The 120 ml starter culture was used to inoculate a 12 l culture the next morning. The protein of interest, expressed under the control of the T7 promoter, was induced with 1 mM isopropyl-

beta-D-thiogalactopyranoside (IPTG) at OD_{600} = 0.6. Cells were harvested after 2 hours by two runs of centrifugation in a Sorvall RC-3B centrifuge equipped with 6x 1 litre swing-buckets at 5,000 rpm for 20 mins, flash frozen in liquid nitrogen and stored at -80 °C until required.

Purification of His-tagged proteins

Cell pellets were thawed in a final volume of chilled 400 ml lysate buffer consisting of 50 mM Tris-Cl at pH 8, 1mM dithiothreitol (DTT), with five Complete EDTA-free protease cocktail inhibitor tablets (Roche, UK), 0.25 mg/ml lysozyme (Sigma, UK) and 0.04 mg/ml deoxyribonuclease 1 (DNAse 1) from bovine pancreas (Sigma, UK). Cells were opened by a cell disruptor (Constant Systems) cooled at 4 °C. The lysate was clarified by centrifugation at 45 000 rpm in a Beckman Coulter Optima L-100 XP Ultracentrifuge, with a Ti45 rotor. The supernatant was loaded onto 2x 5 ml HiTrap HP (Amersham Biosciences, Sweden) and washed thoroughly with 50 mM Tris-Cl, 300 mM sodium chloride, 1mM dithiothreitol (DTT), pH 6. Stepwise elution followed, using the elution buffer consisting of 50 mM Tris-Cl, 1 M imidazole, pH 8. Mal3-His6 eluted predominantly at the 30 % imidazole step. Peak fractions were analysed by SDS-PAGE and desired fractions pooled and concentrated in Centriprep 10,000 MW cut off (Millipore, USA) cassettes centrifuged at 4,000 rpm in an Eppendorf 5810-R benchtop centrifuge to about 2 ml. Imidazole and remaining impurities were removed by size exclusion chromatography with a HiPrep 16/60 Sephacryl S100 HR (for the monomeric constructs) or S200 HR (for the full length proteins) gel filtration column (Amersham Biosciences, Sweden) equilibrated in 20 mM Tris-Cl, 1 mM EDTA, 1 mM sodium azide, pH 7.5. Purified Mal3 ran as a single peak at an elution volume corresponding approximately to the 66 kDa expected for a dimer. Mal3 CH domain constructs ran as single peaks at the elution volume expected for a monomeric 17 kDa

protein (see Fig. 3.3). Tip1-113 ran as a single peak at an elution volume corresponding to a 12 kDa protein. Tip1-205 ran as a single peak at an elution volume corresponding to a 45 kDa protein. It must then be a dimer as expected. A small low molecular weight band always remain with it, even after a further anion exchange column. It must be a cleaved product, probably the dimerization domain (see Fig. 3.3 Right). Peak fractions were concentrated to 20 to 60 mg/ml. Aliquots were flash frozen in liquid nitrogen and stored at –80 °C.

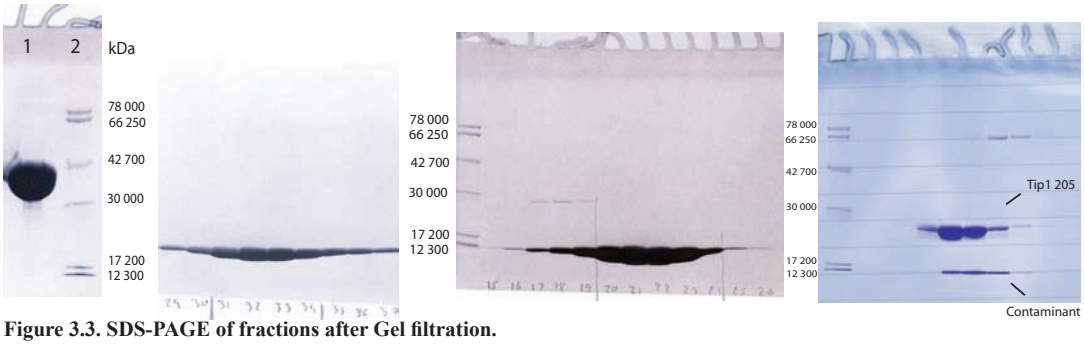

Figure 3.3. SDS-PAGE of fractions after Gel filtration.
Left: 1. Mal3_328. **2.** Molecular Weight Marker (Da) **Middle left:** Mal3_143. **Middle right:** Tip1_113. Left lane: MW (Da). Middle and right bottom: Fractions number. Vertical Marks: Fractions retained. **Right**: Tip1_205 fractions after anion exchange column. Bottom protein contaminant is probably a Tip1 cleavage product. Left: MW (Da).

Expression of GST-tagged protein constructs

E. coli C41 or BL21 strains transformed with GST-Tip1 plasmid vector pOPTG-Tip1 or pGEX-4T1Tip1 were grown as above.

Purification of GST-tagged proteins

Tip1 protein constructs fused with GST tag at their N-terminus were batch purified using Glutathione-Sepharose beads followed by GST cleavage and size exclusion chromatography.

Cell pellets were thawed in a final volume of chilled 400 ml lysate buffer consisting of 50 mM Tris-Cl at pH 8, 1mM DTT, with five Complete EDTA-free protease cocktail

inhibitor tablets, 0.25 mg/ml lysozyme and 0.04 mg/ml DNAse 1. Cells were opened by a cell disruptor (Constant Systems) cooled at 4 °C. The lysate was clarified by centrifugation at 45 000 rpm in a Beckman Coulter ultracentrifuge, with a Ti45 rotor. The supernatant was mixed with 10 ml of Glutathione-Sepharose beads (GE Healthcare) in PBS (140 mM NaCl, 2.7 mM KCl, 10 mM Na_2HPO_4, 1.8 mM KH_2PO_4) and 1% Triton X-100 and mixed for 30 min on a rotary shaker. The beads were then centrifuged and washed four times with PBS. Thrombin or Tobacco Etch Virus (TEV) protease was added either before or after elution from the beads. Tip1 was released from the beads with 10 mM reduced Glutathione in 50 mM Tris-HCl pH 8.0. Eluted Tip1 was then analysed by SDS-PAGE (see Fig. 3.5) and concentrated as above to about 2 ml. Aliquots were flash frozen in liquid nitrogen and stored at –80 °C.

Results

Expression and purification of His tagged Mal3 and Tip1 protein constructs

Protein constructs were fused with a 6 Histidine tag at their C-terminus. They were expressed in *E. coli* under a T7 promoter and purified using nickel-Sepharose affinity chromatography followed by size exclusion chromatography. All protein constructs were very well expressed in *E. coli* and yielded up to 10 mg of protein per litre. They were all obtained to a high degree of purity and soluble in low salt buffer except Mal3-115, which was unstable over 4°C, most probably because the truncation was too extensive, deleting residues of the CH domain fold. Tip1 full length was soluble but very heavily proteolysed (see Fig. 3.4). To circumvent that problem, an attempt was made to express the protein with a cleavable Glutathione S Transferase (GST) tag, as others had succeeded in purifying it by this technique (Brunner & Nurse, 2000).

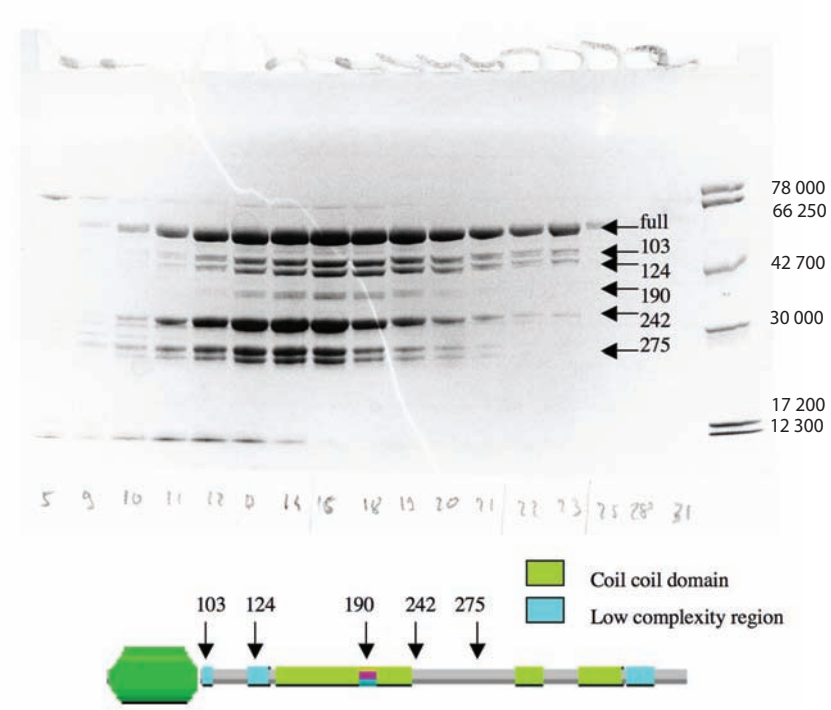

Figure 3.4 Top. Tip1_461-His fractions after anion exchange column. Arrows show fragments with their respective N-terminal 1st amino acid determined by N-terminal sequencing. Fractions number at the bottom. Last lane on the right: molecular weight marker. (Da). **Bottom. Tip1 Pfam graphical.** Arrows show cleavage sites determined by N-terminal sequencing of fragments separated by SDS-PAGE. Cleavage matches with predicted low complexity regions and ends of coiled coils.

Expression and purification of GST-tagged Tip1 protein constructs

GST-Tip1 was well expressed in *E. coli* and did not suffer proteolysis. Although thrombin did not cleave off the GST tag when bound to the beads (Fig. 3.5 top), it did cleave it efficiently after elution (Fig. 3.5 bottom). A major problem arose as thrombin also cleaved off another fragment with the same efficiency as the original thrombin site. Looking carefully at the protein sequence, it appeared that a thrombin site was just in the putative unstructured region between the CH domain and the rest of the protein. The Tip1 sequence was cloned into a pOPTG vector with a TEV site to remove that problem. To complicate things further, the TEV protease did not cleave the GST off this new protein construct. Different constructs will have to be made in the future to resolve that problem. A greater linker length between the GST and the protein may free the way to the TEV cleavage site.

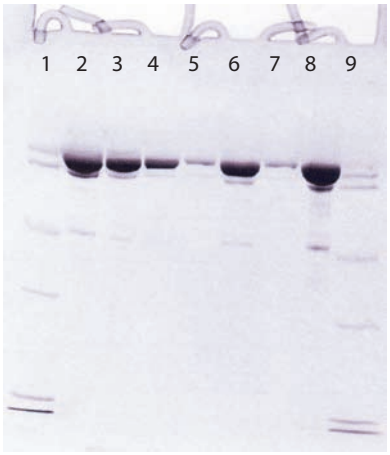

Figure 3.5 Top left: GST-Tip purified on Glutathione S Transferase beads.
Line 1 and 9. Molecular weight markers.
2: Supernatant of the 1st elution with reduced glutathione. **3 and 4:** 2nd and 3rd elutions.
5 to 8: thrombin cleavage trial on the beads.
5 and 7: supernatant. **6 and 8:** bead pellet.
No cleaved protein has been released in the supernatant after overnight incubation with approximately 10 units of thrombin per mg of protein.

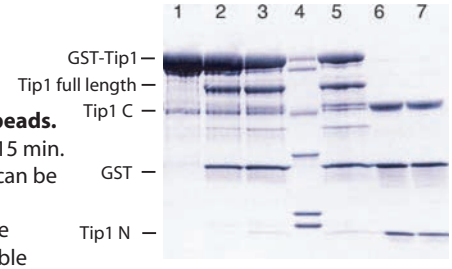

Bottom right: Thrombin cleavage after elution from glutathione beads.
Line 1: no digestion. **2:** 1 min. **3:** 5 min. **4:** molecularweight marker. **5:** 15 min. **6:** 4 h. **7:** Over Night. Three fragments resistant to thrombin cleavage can be seen after overnight incubation. We can resonably think that it is the C-terminal coiled coil, the GST domain and the N-terminal microtubule binding domain. A thrombine cleavage sequence is found in the flexible

Kinesin expression and purification

Tea2 and kinesin-1 T93N (rigor mutant) were made in Rob Cross's Laboratory, MCRI, Oxted.

Kinesin-1 T93N construction, expression and purification were described in Krylyshkina *et al*. (2002).

Tea2 purification was done following the method described in Browning & Hackney (2005).

CHAPTER 4

Characterisation of the +Tips - microtubule interaction

Strategy

Microtubules can be polymerised and stabilised in different ways. Microtubules grow by adding GTP and raising the temperature to 37°C (30°C for *pombe* tubulin) if the tubulin concentration is high enough (15 µM for pig brain tubulin, 5µM for *pombe* tubulin). But the microtubules can be further stabilised by the addition of GMPCPP, a slowly hydrolysable analogue of GTP, or by adding some Taxol, a chemotherapeutic drug that binds and greatly stabilises microtubules. Although it works very well on mammalian tubulin, it is inefficient on *S. pombe* tubulin. Therefore, only GMPCPP was used with *pombe* tubulin.

These compounds have significant effects on microtubules. For example, GMPCPP MTs have a longer dimer repeat compared to GDP MTs (Hyman, Chrétien, Arnal, & Wade, 1995). It is important to perform the pelleting assays in all these different conditions as they might influence the protein binding properties. Also, the protein itself can have an effect on microtubule polymerisation. For example, when tubulin is polymerised with the protein Doublecortin, the proportion of 13 protofilament MTs is greatly increased compared to 14 and 15 protofilament MTs (Moores et al., 2004). Therefore, it is necessary to be careful of the effect that copolymerisation can have on binding properties.

Methods

S. pombe tubulin expression & purification

S. pombe tubulin expression & purification were done by Michael Osei in Rob Cross's laboratory, MCRI, Oxted.

An *S. pombe* strain mmsp174 (*h⁻ ura4.d18 arg3.D4 atb2⁻::nda2⁺*) containing only α1 and β tubulin protein isoforms was created by replacing the *atb2* (α2) gene protein encoding region with the protein coding region of the α1 gene *nda2* using a DNA fragment PCR amplified from genomic DNA. Single isoform α1 and β *S. pombe* tubulin was prepared by a modification of the method of Davis et al. (Davis, Sage, Wilson, & Farrell, 1993) to be described in detail elsewhere. Purified tubulins were desalted into PEM containing 20 μM GDP before storage in liquid nitrogen. Protein concentrations were determined by UV absorption scan of protein samples dissolved in 6 M guanidine hydrochloride, assuming full nucleotide occupancy and ε of 108,390 M-1 cm-1.

Pig brain tubulin purification

Native pig brain tubulin was purified by successive cycles of temperature-dependent polymerization and depolymerization as described by Castoldi et Popov (Castoldi & Popov, 2003)

After the standard glycerol cold-warm cycles, 15ml of glycerol microtubules were incubated on ice with 10ml 1 M PIPES/KOH pH6.9 for 20 minutes. The sample was centrifuged at 42,000 rpm, 4 °C for 60 minutes; 10% DMSO and 20% glycerol were added to the supernatant, which was incubated at 37 °C for 30 minutes. Polymerized tubulin was centrifuged at 40,000 rpm at 30 °C for 60 minutes. The pellet was resuspended and mixed with a hand-homogeniser in 2ml ice cold column buffer (0.1 M PIPES pH

6.9, 1mM $MgSO_4$, 1mM EGTA, 1mM DTT). Purity of protein was checked by SDS-PAGE, concentrated to 10mg/ml using the Vivaspin 10,000 Da molecular weight cut-off concentrators (VIVASCIENCE), flash frozen and stored in liquid nitrogen.

MT pelleting assays

For GMPCPP prepolymerized MT binding assay, 5 to 8 μM of pig brain tubulin in BRB80 (80 mM K-PIPES, pH 6.8, 1 mM $MgCl_2$, 1 mM EGTA, 1 mM DTT) and 2 mM GMPCPP was incubated on ice for 5 min and then at 30 °C for 30 min. 40 μl of prepolymerized MTs were mixed with the protein of interest diluted at various concentrations in BRB80 and incubated for 10 min at 30 °C.

For prepolymerized Taxol stabilised MT binding assay, 5 to 8 μM of pig brain tubulin in BRB80 and 1 mM GTP was incubated on ice for 5 min and then at 30 °C for 30 min. Taxol was added slowly to a concentration of 10 μM. 40 μl of prepolymerized MTs were mixed with the protein of interest diluted at various concentrations in BRB80 and incubated for 10 min at 30 °C.

For copolymerization and binding assay, 50 μl mixtures of 5 to 8 μM tubulin and the protein of interest at various concentrations were mixed on ice in BRB80, 1 mM GTP or 2 mM GMPCPP and incubated for 5 min, then at 30 °C for 30 min.

All samples were centrifuged at 50,000 rpm, 30 °C for 5 min in a TLA100 rotor using an Optima TLX ultracentrifuge (Beckman Coulter). The pellet fractions were resuspended in 50 μl of BRB80 buffer. Pellet and supernatant fractions were analysed by SDS-PAGE using 12.5% Tris-HCl Bio-Rad Criterion Precast gel. Gels were stained with Sypro Red (Invitrogen) following the manufacturer's instructions and the fluorescence

images of the gels were recorded using a Molecular Imager FX (Bio-Rad). Protein bands were quantified using Quantity One software (Bio-Rad) within the linear signal intensity range.

Results

Mal3 binds to MTs in a one to one ratio to tubulin dimers

Sedimentation assays using *S. pombe* MTs showed stoichiometric binding of Mal3_143 to the MT lattice, with saturation at a ratio of one Mal3_143 monomer per tubulin heterodimer and a fitted Kd of 2.4 ± 0.9 (s.e.) μM. (Fig. 4.1 right). The dimeric construct, Mal3_308 also bound at a ratio of one Mal3 molecule per tubulin heterodimer, with a 2.4-fold tighter Kd (0.9 ± 0.3 μM) (Fig. 4.1 left). Such a difference between the monomer and the dimer is expected as the dimer has twice as many MT binding sites compared to the monomer. It was very surprising, however, to see a different binding stoichiometry compared to that reported by Sandblad et al. (2006). In their article they described an experiment where they obtained a ratio of 1 Mal3 per 9 tubulin heterodimers, which they correlated with their observation by EM that Mal3 decorated the MT only along the seam. This was in complete disagreement with the results described here. A careful examination of both sets of experiments had to be done to reveal what caused this difference.

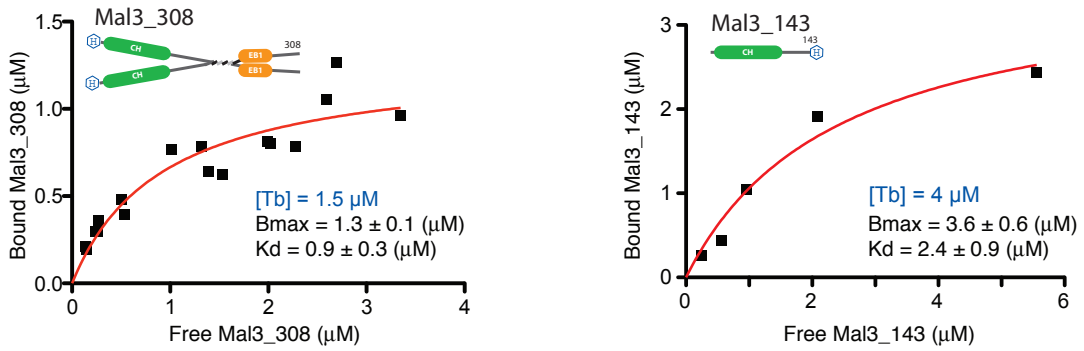

Figure 4.1 Mal3 interaction with MTs in vitro.
Binding of Mal3_308 or Mal3_143 to GMPCPP stabilised MTs. Mal3 was incubated in K-PEM, 30 mM NaCl, 1mM GMPCPP, 1mM AMPPNP-Mg2+ with 4µM of prepolymerized *S. pombe* MTs. After pelleting and quantification by SDS-PAGE, the concentration of Mal3 bound to MTs was plotted against the concentration of unbound Mal3. Data points were fitted by least squares using a rectangular hyperbola with the program PRISM (GraphPad software). **Top of each graph.** Domain structure of Mal3 constructs used in these experiments. Calponin homology (CH) and EB1-like C-terminal motif domains are indicated by green and orange, respectively. Boundaries for each domain are indicated by residue numbers. 6xHis-tags are highlighted in blue.

Mal3 binds tighter to co-polymerised MTs

In their experiment, Sandblad et al. prepolymerised brain MTs and stabilized them with Taxol. They subsequently mixed them with Mal3, incubated 10 min at room temperature and centrifuged (Sandblad et al., 2006). In my experiments, I mixed Mal3 with either *pombe* or pig brain tubulin on ice and then co-polymerised them at 30°C for 30 min and centrifuged. The type of tubulin used did not seem to have an obvious effect on Mal3 binding. The other obvious difference between the experiments was that they had prepolymerised and Taxol stabilized their MTs while I had copolymerised them with Mal3. Some MAPs influence MT structure (Moores et al., 2004) or bind differently to co and pre-assembled MTs (Kar, Fan, Smith, Goedert, & Amos, 2003). Therefore, this is the most obvious difference that might explain the conflicting results. Taxol may also have an effect on MAP binding. It could compete for binding sites but is also known to have drastic effects on MT polymerisation, stability and structure. It was important to check all these parameters independently.

To fix the tubulin parameter, pig brain tubulin was used for the next set of experiments.

The influence of co versus pre-assembling the MTs was then tested with either Taxol or GMPCPP as stabilizer. The result showed unambiguously that Mal3 bound up to 3-fold tighter to co-assembled MTs compared to pre-assembled MTs (Fig. 4.2).

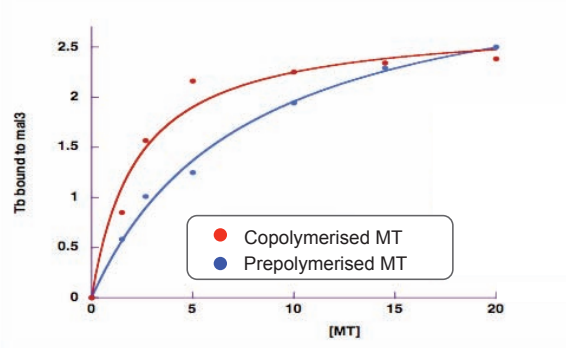

Figure 4.2 Difference between Pelleting assay of Mal3 co-assembled and pre-assembled with tubulin
2.5 μM Mal3_308 was either co-assembled with pig brain tubulin (35ºC 10min then 25ºC for 20 min) or mixed with preassembled pig GMPCPP-stabilised MTs (10min 25ºC) in K-PEM supplemented with 10 mM NaCl, 1mM DTT, 1mM GMPCPP. Samples (50μl) were pelleted in TLA100 rotor, 5min, 50000 rpm, 25ºC. Pellet and supernatant fractions were analysed by SDS-PAGE. Pelleting assays with Taxol stabilized MTs gave similar results as the ones with GMPCPP MTs.

Whether the MTs were preassembled with GMPCPP or Taxol did not make any difference. Mal3 affinity was exactly the same for the two stabilization methods. Taxol does not compete with Mal3, therefore the Mal3 stabilization mechanism does not seem to involve the tubulin M loop (Nogales, Whittaker, Milligan, & Downing, 1999). At the same time, the experiment does not show any increase in binding affinity with GMPCPP. This would imply that Mal3 tip tracking behaviour is independent from the GTP cap that GMPCPP should mimic. Maybe GMPCPP stabilizes MTs without exactly mimicking the GTP cap. Or Mal3 may bind with high affinity to the GDP.Pi state that could be different from the GTP state. This would reconcile the Dreischel et al. finding that the GTP cap itself may only be a single ring of GTP tubulin (Drechsel & Kirschner, 1994) and the data of Bieling et al. who observed that Mal3 binds with high turnover on a tip structure that lasts for 8 secs (Bieling et al., 2007). These 8 secs could be the time needed for the Pi to be released from the MT lattice. In any case, we can conclude that Mal3 must have an important effect on MT structure when copolymerized with tubulin, and that difference in MT structure affects its own binding.

Does Tip1 bind to microtubules?

Studies have found that the Tip1 homologue Clip-170 binds strongly to tubulin dimers and to microtubules in vitro (Diamantopoulos et al., 1999) (Folker et al., 2005). The main difference between Clip-170 and Tip1 is in their respective CAP-Gly domains, thought to be their MT binding domains. Clip-170 has two CAP-Gly domains whereas Tip1 has only one. With such a difference, does Tip1 have the same behaviour as Clip-170? It has been found that Tip1 can bind to MTs in vitro (Brunner & Nurse, 2000). On the other hand, Bieling et al. did not observe much binding in conditions where Mal3 was tip tracking (Bieling et al., 2007). In my hands, it has been hard to get a definite answer. By pelleting assay, there was definitely not a strong binding but it is difficult to conclude whether there is a weak binding or no binding at all. (see Fig. 4.3). Pelletting assays suffer from the fact that proteins are adsorbed on the tube walls, thereby compromising the result's accuracy. It is therefore difficult to measure weak interactions. It has been shown that tubulin's C-terminal tyrosination state is very important for Clip-170 binding (Peris et al., 2006). I did not have control over that in my experiments and it might be important for Tip1 binding.

Figure 4.3 Pelleting assays of Tip1_113 with pig brain tubulin.

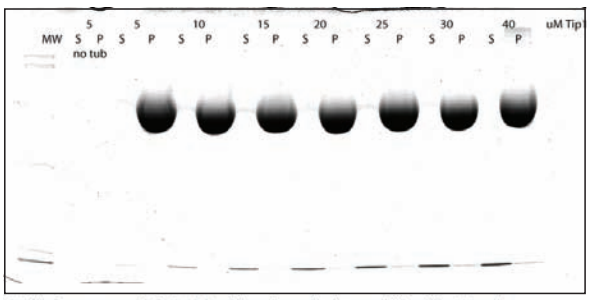

Pelleting assay of Tip1 with microtubules stabilized by Taxol. Tubulin concentration is 10 μM. Tip1 concentration from 5 to 40 μM.

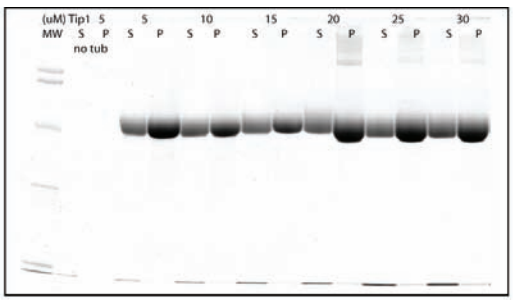

Pelleting assay of Tip1 with unstabilized microtubules. Tubulin concentration is 10 μM. Tip1 concentration from 5 to 35 μM.

Tea2 interacts with MTs and competes with Mal3

Tea2 or rat kinesin-1 displaces Mal3 from the MT (see Fig. 4.4). This means that they are likely to have overlapping binding sites. As most of the Mal3 proteins are displaced, the kinesins must have a stronger affinity for the MT. But as a small proportion of Mal3 protein seems to remain attached, the binding sites may not be completely overlapping. It cannot be concluded from this experiment that Mal3 binds one tubulin subunit or the other, since the kinesin motor is quite big and may still impede Mal3 binding to either the α subunit or the β subunit. If Mal3 binds in the groove between protofilaments (Sandblad et al., 2006), it is likely to make contacts with tubulin subunits on the two protofilaments. So even if its main binding site is on an α subunit and quite distinct from kinesin's site, as suggested by Richards et al. (2000), its proper binding could be hampered by a kinesin bound to a subunit of the opposite protofilament.

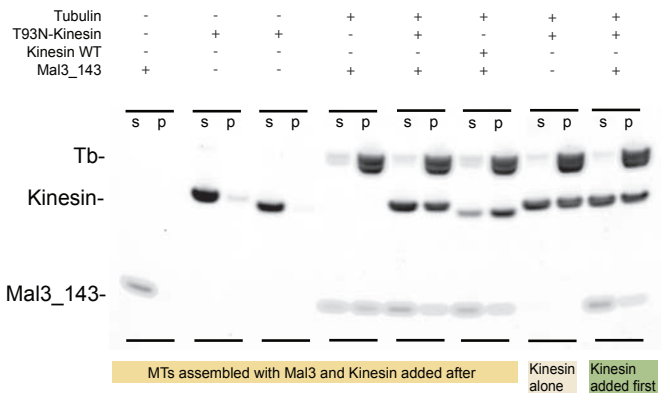

Figure 4.4a Competition assay between Kinesin and Mal3_143.
5 µM Mal3_143 and 5 µM *S. pombe* tubulin were mixed in BRB80 containing 4mM GMPCPP , 1mM DTT, 2 mM AMPPNP on ice for 5min then incubated at 30ºC for 10 min. 7 µM rat kinesin-1 K340 (wildtype or T93N) was added, and incubation continued for 5 min before centrifugation. Alternatively, the kinesin and tubulin were mixed first on ice 5min then incubated at 30ºC for 10min before addition of Mal3_143 and incubation for 5min before centrifugation of 50µl in TLA100 rotor, 5min, 50000 rpm, 30ºC . After separation by SDS-PAGE the quantities of Mal3_143, kinesin and tubulin were measured. S and P indicate supernatant and pellet fractions, respectively.

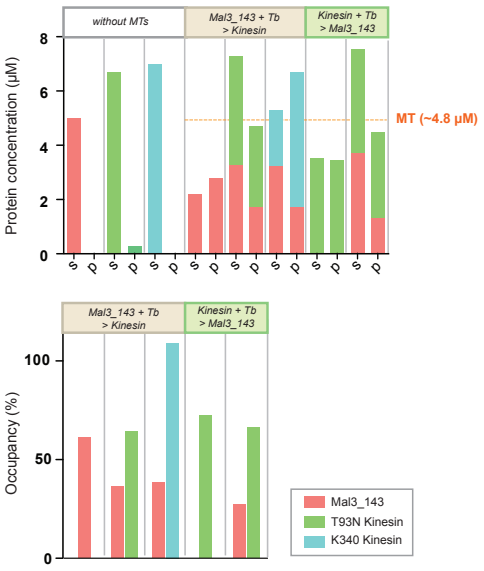

Figure 4.4b Competition assay between Kinesin and Mal3_143
Upper histogram shows the tubulin, Mal3_143 and kinesin content of the pellet and supernatant fractions. The lower histogram shows the percentage occupancy of the MT lattice by Mal3_143 and kinesin in each sample, assuming one Mal3_143 and one kinesin binding site per tubulin heterodimer in the MT pellet. The partial displacement of Mal3_143 by kinesin binding suggests that the binding sites of both proteins either partially overlap or are close enough for kinesin to cause steric hindrance of Mal3_143 binding.

CHAPTER 5

Measuring +Tips effect on MT dynamics by light scattering and DIC microscopy

Strategy

The difference in scattering properties between tubulin in solution and polymerised into microtubules gives the possibility to follow the amount of tubulin polymerised as a function of time in a relatively simple and quick manner. It also allows one to follow in real time the effect of added proteins or reagents or temperature changes. Several different conditions can be measured within a day.

Video-enhanced differential interference contrast microscopy (VE-DIC microscopy) is also a powerful way to follow sub resolution objects, like microtubules, in real time and therefore to gain insight into kinetic parameters of individual MTs. This method was applied to study the effect of +Tip tracking proteins on MTs growth and shrinkage rates as well as frequency of catastrophe and rescue events.

These experiments were done in the laboratory of Dr R. A. Cross (MCRI, Oxted), in collaboration with Dr. M. Katsuki, in order to assay the activities of proteins I had prepared in Cambridge (see Chapter 3)..

Methods

Light scattering

4 μM of *S. pombe* tubulin and various concentrations of Mal3 constructs were mixed on ice in K-PEM buffer containing 1 mM DTT, 1 mM GTP and transferred to a quartz

fluorimeter cuvette temperature-controlled to 25 °C by a Cary single cell Peltier heater. Scattering of 350 nm wavelength light at 90° angle was recorded in a Cary Eclipse Fluorescence spectrophotometer. After 30 min incubation, samples were immediately transferred onto poly(L-lysine) coated slide glass and observed by video enhanced DIC microscopy using a CCD camera C3077 and Argus video processor (Hamamatsu Photonics) to check if the scattering was effectively due to MTs.

Assay of assembly dynamics by VE-DIC

Method adapted from Walker et al (Walker et al., 1988) by Douglas Drummond and Miho Katsuki (MCRI, Oxted). Mal3_308/MT tip tracking and data plot were performed by Miho Katsuki.

Flow cells were made with a clean slide, covered with a clean 22-mm^2 coverslip (thickness No. 1.5), and then sealed with Valap (1:1:1 mixture of Vaseline (petroleum jelly): Lanolin (Sigma L-7387, wool fat): soft paraffin wax (Agar L4182, low temperature wax 45^{o}C).) to prevent drying and to prevent flow within the slide-coverslip chamber.

The flow cell was filled with a preparation of axonemes from sea-urchin sperm (*Echinus esculentus* , prepared by Douglas Drummond) diluted in K-PEM pH 6.9 (100mM PIPES, 1mM $MgSO_4$, 2mM EGTA adjusted to pH 6.9 at 25^{o}C with KOH) and 5 minutes at room temperature for the axonemes to stick to the surface. An appropriate axoneme concentration should give 2-3 axonemes per field of view. The flow cell was then washed with 5 cell volumes of K-PEM, 1 mM GTP and DTT. The flow cell was filled on ice with the sample preparation containing typically 3 μM *S. pombe* tubulin in K-PEM, 1 mM GTP, 1 mM DTT and other proteins or compounds at the desired concentration and then warmed to 30°C on the microscope stage to induce assembly.

Preparations were viewed by differential interference contrast (DIC) microscopy, using a Nikon (Microphot-SA) microscope equipped with DIC prisms, [1.4 NA condenser,

and 60X/1.4 NA DIC Plan Apo lens]. An HBO mercury lamp (Osram) provided full illumination of the condenser aperture via a fibre optic light scrambler (Technical Video) through heat-cut and 546-nm interference filters. Images were captured by a CCD camera C3077 Hamamatsu]. Images were further enhanced using an Argus 10 (Hamamatsu Corp.) image processor for real-time background subtraction and two frame averaging. Images were recorded onto super VHS video tapes using a Panasonic AG 7350 recorder. Movies were digitized frame by frame using an LG3 video capture card (scion corp) and analyzed using Image J. A point cursor was used to track the end of the microtubule. Data points were taken by manually positioning the cursor with a mouse. Changes in microtubule length were plotted as a function of time in Kaleidagraph, and the average rates of elongation and rapid shortening were determined by least squares regression analysis.

Results

Light scattering assembly assay using Mal3 constructs

When the tubulin concentration was below the critical value for self-assembly, Mal3 strongly promoted MT assembly (Fig. 5.1). Recently published data indicate that human EB1 does not affect MT growth rate, but can suppress catastrophe and shrinkage rates (Manna, Honnappa, Steinmetz, & Wilson, 2008). With *S. pombe* tubulin, Mal3 was found to drive polymerization, with the rate and extent of polymerization dependent on the concentration of Mal3 (Figs 5.1 and 5.3). MT assembly was also promoted by the first 143 N-terminal amino acids alone (Mal3_143, Fig..5.1), that is, the globular Calponin Homology (CH) domain plus a 40-residue tail, predicted to be mainly unstructured (Honnappa et al., 2005).

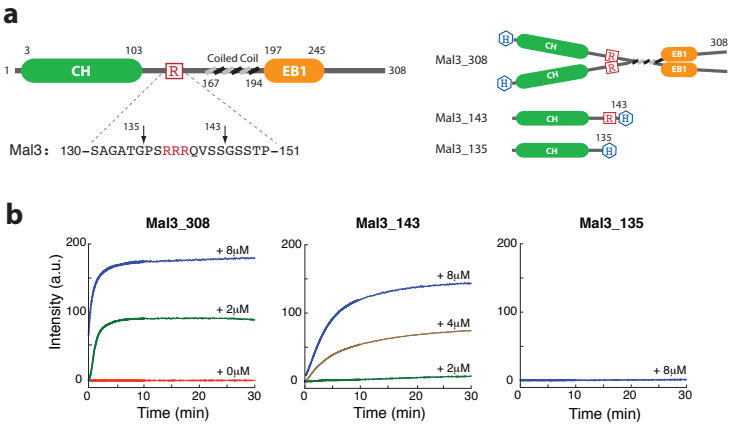

Figure 5.1 Mal3 promotes tubulin assembly.
a, Domain structure of Mal3. Calponin homology (CH) and EB1-like C-terminal motif domains are indicated by green and orange, respectively. Boundaries for each domain are indicated by residue numbers. The amino acid sequence for residues 130-150 is shown below and the three arginine residues are highlighted in red. Right, domain structure for the constructs used in this study. 6xHis-tags are highlighted in blue. **b,** MT polymerization assay by 90° light scattering at λ = 350 nm. All assays contained 4μM *S. pombe* tubulin (dimer concentration). Coloured lines indicate the added Mal3 monomer concentration; red, 0 μM; green, 2 μM; brown, 4 μM; blue, 8 μM.

This truncated molecule was monomeric by gel filtration (Fig. 5.2), showing that dimerisation of Mal3 is not a requirement for MT stabilization. The full-length protein was nonetheless a more potent nucleator (Fig. 5.1). Deletion of a further 8 residues from the C-terminus of Mal3_143 (to create Mal3_135) abolished its polymerization-enhancing activity. Interestingly, this 8-residue region contains a 3-residue polyarginine sequence, suggesting a possible electrostatic role for this functionally critical region.

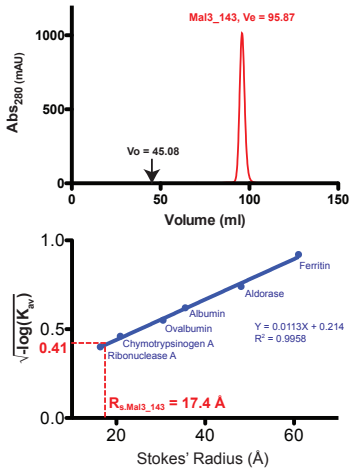

Figure 5.2 Gel filtration of Mal3_143
Mal3_143 was analysed by gel permeation chromatography on a Superdex 200 16/60 pg column (GE Healthcare) in an Akta purifier 10 system (GE Healthcare) in 20 mM Tris pH 7.4, 400 mM NaCl at 4oC. The column was calibrated using protein standards of known Stokes' radius (GE Healthcare) and a standard curve of (-log-Kav)1/2 plotted against Stokes' radius. Mal3_143 eluted as a single peak in a volume equivalent to a Stokes' radius of 17.4 Å. This is close to the Stokes' radius of 20.5 Å predicted for the calculated molecular weight of Mal3_143 (mw 17, 486) using the relationship determined by Uversky (1993) for a range of native proteins, and is consistent with Mal3_143 protein being a monomer.

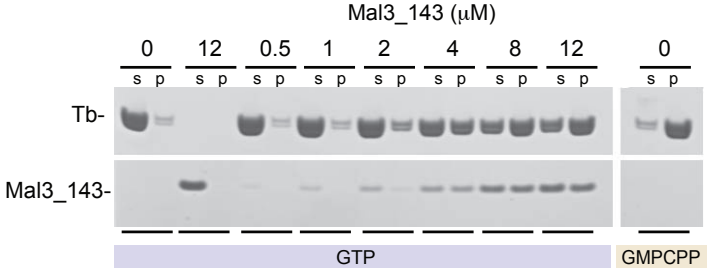

Figure 5.3 | Pelleting assay of Mal3 co-assembled with tubulin
Mal3_143 (0 – 12 μM) and 8 μM of *S. pombe* tubulin were copolymerized in the presence of 1 mM GTP and pelleted. S and P indicate supernatant and pellet fractions, respectively. More tubulin assembles when more Mal3 is added and more Mal3 is also pelleted until the MT dimer lattice becomes saturated.

DIC dynamics assay using Tip1 and Mal3

With the protein Tip1, either monomeric or dimeric, no effect on MT dynamics was observed. All parameters were indistinguishable from the control with tubulin alone. Mal3 on the other hand had a very obvious effect. Around stoichiometric quantities of Mal3, MTs were so long and stable, even before they could be put under the microscope, that no kinetic parameters could be recorded. By lowering Mal3 concentration down to about one tenth of tubulin concentration and being very quick to start imaging the sample, it was possible to see that Mal3 was drastically stabilizing MTs. MTs would grow continuously from both ends up to lengths which could not be followed any more on a single field of view. Looking carefully at the kinetic parameters, it was clear that the MT growth rate was left unchanged but catastrophes were completely suppressed. This fits with a model where Mal3 does not associate with free tubulin to help it assemble into MTs but only binds to assembled MTs or sheets and stabilizes their structure.

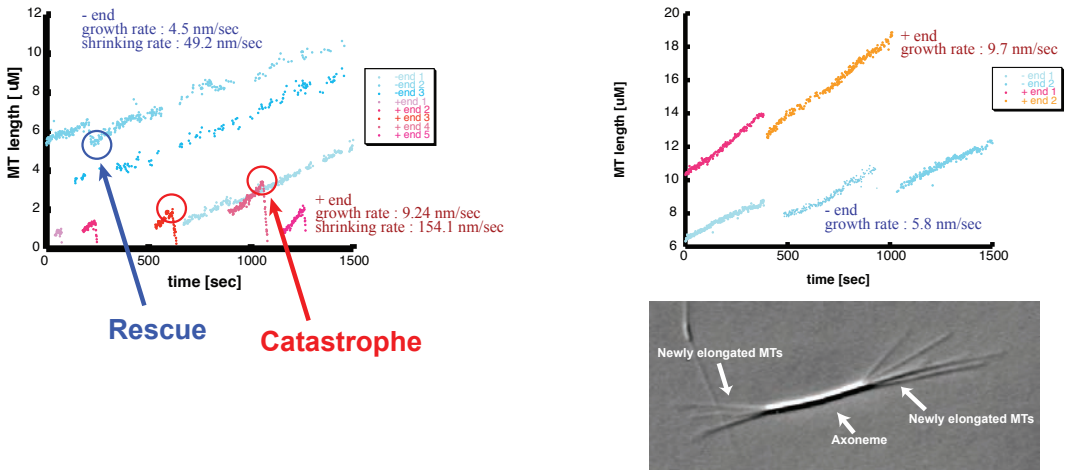

Figure 5.4 VE-DIC microscopy measurement of Mal3 effect on MT polymerization dynamics. In blue: minus end dynamics measurement, in red: plus end dynamics measurement. Mal3 suppressed the catastrophe frequency at plus ends, without any significant effect on the growth rate. Bottom: VE-DIC image of microtubules nucleated by an axoneme.

CHAPTER 6

Decorating MTs with Mal3 monomer and studying the complex by electron microscopy

Strategy

As Mal3 was found to bind in a one to one ratio with tubulin dimers in MTs, it was relevant to study the structure of Mal3 decorated MTs by helical 3D image reconstruction methods. As a difference in affinity had been found depending on whether Mal3 was coassembled with MTs or whether it was bound to MTs after assembly (see Chapter 3), it was decided to proceed by coassembling Mal3 with MTs prior to staining or freezing on the EM grid.

Helical symmetry

13 or 14 protofilament (pf) MTs have a 3 tubulin monomer helical pitch. In an EM image of a bare MT, α and β tubulin subunits are indistinguishable at 10 or 20 angstroms resolution. Therefore MTs can be considered helical assemblies of tubulin monomers and helical symmetry can be applied to reconstruct their structure in 3 dimensions. But if a protein decorates the microtubule lattice by binding to one or the other tubulin subunit, tubulin subunits are not indistinguishable any more. One has a protein bound to it and the other not. The microtubule lattice has then to be regarded as a lattice of tubulin dimers and the helical pitch of 3 monomers is now a pitch of one and a half dimers. Therefore, 13 and 14 pf MTs with a B lattice are not truly helical and have a discontinuity called the seam where tubulin heterodimers are shifted by half a dimer

(see Chapter 1).

To circumvent that problem, one can seek for MTs with more than 14 pfs, which can have a pitch of four tubulin monomers (two heterodimers) and therefore are truly helical. In vivo, MTs almost only have 13 pfs. Their diameter must be tightly controlled by many cellular factors. In vitro, MT assembly is polymorphous, with a similar number forming 13 and 14 pfs, and a smaller proportion of 15 and 16 pf MTs (less that 10 %). It is known that for pure brain tubulin this proportion can be increased by adding 10 % of DMSO to the polymerisation buffer.

Methods

Negative staining of Mal3 bound to MTs

5 µM of *S. pombe* tubulin and 6 µM of Mal3_143 were mixed in BRB80 with 1 mM GTP and left on ice for 5 min. Then polymerisation was induced by incubating at 30 °C for 15 min. The sample was applied on an EM grid coated with a carbon film and then negatively stained with uranyl acetate, blotted and dried. Pictures were taken in a Philips 208, 100 kV microscope running at 80 kv. The images were photographed with Kodak SO-163 film at 50,000 magnification with a defocus of 1–3 µm and digitized in 6 µm steps using the MRC-KZA scanner.

Kinesin decoration

Kinesin decoration experiment was done by co-assembling 5 µM *S. pombe* tubulin with 10 µM kinesin in BRB80, 1mM AMPPNP and 1 mM GMPCPP at 30˚C for 15 min, or by coassembling 6 µM Mal3 with 5 µM *S. pombe* tubulin in BRB80, 1 mM AMPPNP and 1 mM GMPCPP and subsequently adding 10 µM kinesin. Samples were then applied on a carbon-coated grid, washed with BRB80 and negatively stained with 1% uranyl acetate.

Electron cryo-microscopy of Mal3-MT

5 µM of *S. pombe* tubulin and 6 µM of Mal3_143 were mixed in BRB80 with 1 mM GTP and left on ice for 5 min. Then polymerisation was induced by incubating at 30 °C for 15 min. The sample was applied on an EM grid coated with a holey carbon film and rapidly frozen in liquid ethane. The grids were examined by using a Gatan cold stage in a FEI F20 electron microscope operating at 200 kV. The images were photographed with Kodak SO-163 film at 50,000 magnification with a defocus of 1–3 µm and digitized in 6 µm steps using an MRC-KZA scanner.

Image analysis

Cryo-EM images were processed using the MRC package of programs (Crowther et al., 1996); images were boxed, floated and fast-Fourier-transformed. Layerline data were selected (see Figs 6.4 and 6.5) and averaged, and a 3D map at ~2nm resolution was calculated by Fourier-Bessel transformation.

Results

Negative stain study of Mal3 dimers and monomers bound to MTs

Images taken of negatively stained MTs decorated with Mal3 did not produce a decoration pattern directly visible on the MT wall. This must be mainly because Mal3 is a small protein, therefore difficult to see directly, especially if it is sitting in the groove between protofilaments. To see if there was a decoration pattern on the microtubule lattice, the Fourier transforms of individual MT images were calculated. The resulting intensity patterns showed the usual 1/4 nm layerline corresponding to the tubulin subunit repeat. When images were of good enough quality, the Fourier pattern also displayed

an 1/8 nm layerline that would not be seen with tubulin alone. This layerline could only be explained by Mal3 decorating the microtubule lattice every 8 nm. This was in agreement with the sedimentation assays showing Mal3 binding in a one to one ratio with tubulin heterodimers and in agreement with published heavy metal shadowing images (Sandblad et al., 2006).

There were sometimes also additional layerlines at 1/16 and 1/32 nm, not fitting with the usual MT lattice. These layerlines of longer repeat length could only be explained by a repetitive arrangement of Mal3 C-terminal coiled-coil. If the two MT binding domains were often binding at an 8 nm distance from each other, each dimer coiled coil domain would then be 16 nm from the next, producing a 1/16 nm layerline on the diffraction pattern. If they were binding at 16 nm from each other, they would produce a layerline at 1/32 nm. In reality, there must be a mix between many different conformations, with Mal3 dimers binding with different spacing and different orientations, and producing many different layerlines difficult to interpret. A way to make these diffraction patterns simpler was to remove the C-terminal dimerisation domain by using Mal3 MT binding domain alone. As Mal3_143 binds MTs with similar affinity and has similar microtubule stabilization properties, it was relevant to use it for this study. As expected, diffraction patterns of MTs decorated with Mal3_143 only displayed layerlines at 1/4 and 1/8 nm and were therefore easier to interpret. The 1/8 nm layerline had a similar intensity compared to the previous ones, showing that this shorter protein construct decorated MTs just as well. Negative staining thus demonstrated that Mal3 decorated MTs and that the MT-Mal3 complex was a suitable specimen for structural analysis by electron cryo-microscopy and helical 3D image reconstruction.

Finding the right specimen for helical 3D image reconstruction

The aim was to reconstruct a 3D image of a MT fully decorated with Mal3_143, in order to gain insight into the effect of Mal3 on MT structure. The first images taken by cryo-EM showed that Mal3 was still producing a clear 8 nm layerline in MT diffraction patterns. The sample seemed therefore suitable for helical 3D image reconstruction, provided that MTs with helical symmetry could be found.

Effect of DMSO

When MTs were polymerised in the presence of DMSO, it was not possible to find any MT well decorated by Mal3. The 8 nm layerline was always absent and the search for good specimens was further complicated by the fact that the ice was always very dark or even black and bubbling, because of DMSO's higher density to electrons. This is generally overcome by diluting ten times the sample before applying it on the grid. Diluting the sample ten times would bring Mal3 concentration to 0.6 μM, and as Mal3 binds to the MT with approximately 3 μM affinity, it would be stripped off the MT by such treatment. Quickly rinsing the grid before freezing it, in the hope of diluting the DMSO before the Mal3 could come off, was unsuccessful for getting a good MT decoration. Therefore DMSO was omitted from the polymerisation buffer in the expectation that about 10 % of the MTs should still have more than 14 pfs.

MT concentration on the grid

The first grids were full of MTs because the sample was applied undiluted. MTs were on top of each other and only on rare occasions could isolated stretches be analysed. Diffraction patterns of these MTs showed a good Mal3 decoration but the images were mostly too short for further analysis because of other MTs crossing their path. Diluting

the sample, even slightly, gave very poor decoration patterns. Undiluted samples were washed with purified water on the grid just before plunging them in liquid ethane, relying on the greater strength of electrostatic interactions in the low ionic strength of pure water to keep the Mal3-MT complex together. This method gave some good results but the decoration was often very variable, with some grids having completely bare MTs. In the end, there was no better technique than to apply the sample undiluted on the grid, search for regions with a reasonably low density of MTs and hope to find long enough stretches of MTs for diffraction analysis.

Looking for 15 pf MTs with helical symmetry

The number of pfs a MT has can be reasonably guessed by the Moiré pattern made by the pfs and by looking at the MT edges. MT edges can show whether the pf number is odd or even. If it is even, the MT edges on both sides will have a similar thickness whereas if it is odd, one side will appear thicker than the other (see Fig. 6.1). The Moiré pattern reflects the protofilaments super-twist. With 13 pf MTs, pfs run straight relative to the long axis of the MT and can be followed by eye over a long distance on the MT. With 14 or more, the protofilaments have a supertwist. They do not run straight along the MT axis. The result is that protofilaments at the front and at the back, depending on their position along the length of the MT, will either be on top of each other, therefore reinforcing their signal, or be out of register, therefore cancelling each other. This will give a Moiré pattern where pfs will be clearly visible on a short stretch, then will fade away, then appear again and so on, with a longitudinal repeat between each phase depending on the amount of super-twist. By combining these two sets of information, the MT pf number can be reasonably assessed (Wade & Chrétien 1999). However, it was impossible to identify any MTs with 15 pfs. As more pictures were analysed, it became clear that there was not a single MT with a Moiré pattern exhibiting the

short longitudinal repeat characteristic of MTs with more than 14 pf. Every specimen appeared to twist very slowly, giving the pfs a very long helical pitch. Helical 3D image reconstruction seemed impossible because of the lack of helical specimens, even after almost a thousand MTs had been investigated. One way to get around that would be to use a real-space back-projection method (Dias & Milligan, 1999). When a MT such as a 14 pf MT has a super-twist, all the views of that MT are available, providing that it is long enough to have at least one full turn of super-twist. One can therefore divide it in small segments and align them to reconstruct a 3D image of that MT.

Figure deleted in the published version for copyright reasons.
See wade and chretien for the original work.

13-protofilament MTs with mixed lattices

It seemed worthwhile to look for well-decorated MTs with a super-twist. In order to do that, MTs with a Moiré pattern were identified and their Fourier transforms calculated to check if they had a strong 8 nm layerline. However, it proved difficult to find MTs displaying a clear Moiré pattern. Most of them seemed to be fairly straight, with no or

only a very slight super-twist. It appeared that the majority were 13 pf MTs. Moreover, their diffraction patterns were often strange. Many spots on the 8 nm layerline were not at the usual place seen with kinesin decorated MTs. Looking carefully at more of these diffraction patterns, it gradually appeared that the additional spots could only be explained by a partial A lattice arrangement of the tubulin dimers. And with a few MTs, the diffraction pattern showed only spots corresponding to an A lattice (see Fig. 6.2).

To check that the A-lattice patterns really arose from the underlying tubulin lattice rather than from only partial decoration with Mal3, tubulin was copolymerized with Mal3_143 and subsequently added to monomeric kinesin, which bound stoichiometrically [displacing some of the Mal3_143, as determined by a pelleting assay (Fig. 4.3)]. The pattern of kinesin decoration was first examined directly by negative staining. MTs assembled from tubulin alone and decorated with monomeric kinesin clearly had the typical B-lattice, with lines of kinesins on the MT wall at about 10 degrees to the horizontal axis (Fig. 6.2e). MTs coassembled with Mal3_143 typically displayed lines on the MT wall at a higher angle (Fig. 6.2f). Fourier transforms of the images confirmed that the former have a B lattice and the latter mixed lattices (Fig. 6.2g,h), indicating that the mixed or A-lattice patterns were due to the underlying tubulin subunit arrangement. Such patterns were not restricted to MTs assembled from *S. pombe* tubulin. Experiments with brain tubulin coassembled with *S. pombe* Mal3_143 also produced MTs with mixed lattices (Fig. 6.3).

These results were very surprising as there is a general belief that MTs only assemble into the B lattice form in BRB80, the standard buffer for assembly in vitro. Mixed lattices, described as lattices with multiple seams, have only been seen before in high salt conditions (Dias & Milligan, 1999). These unexpected results show that Mal3 not only drives strongly towards assembly of exactly 13 protofilament MTs, as does doublecortin, another lattice stabilizing MAP, but also drives towards the assembly of A-lattice MTs, which has not been seen before.

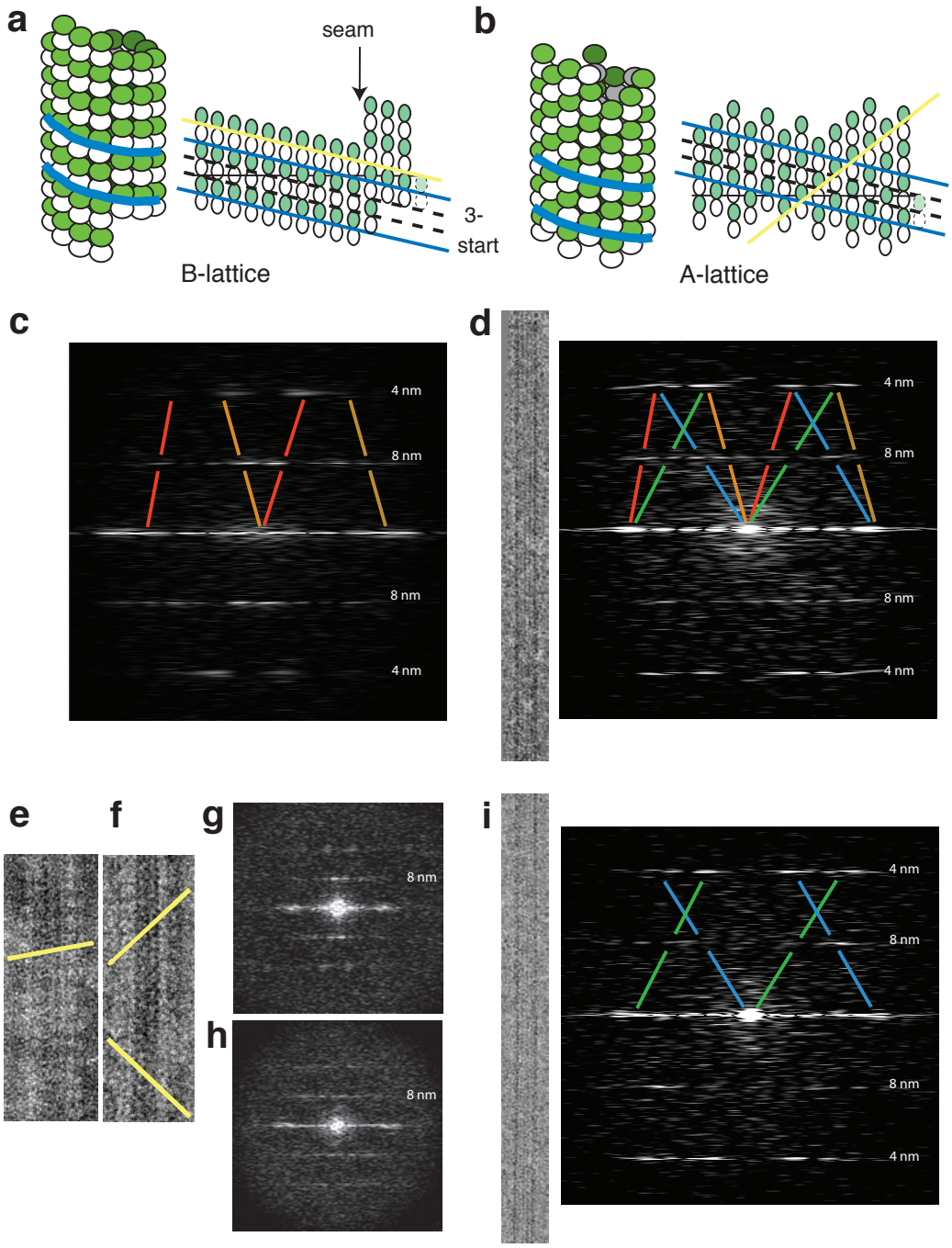

Figure 6.2 MTs assembled with Mal3 show mixed lattices.
a, b, Diagrams of MTs with A and B lattices of tubulin heterodimer subunits, represented both as 3D MTs and as opened-out sheets. White subunits, alpha-tubulin. Green subunits, beta-tubulin. Blue lines, the direction of the 3-start family of helices, common to both lattices, that arises because subunits in adjacent longitudinal protofilaments are staggered by 0.9nm. Yellow lines, the directions of the decoration patterns, different on both lattices, as shown in e and f. **c,** Diffraction pattern from a cryo-EM image of a pure tubulin MT decorated with kinesin head domain. Red and orange lines show the B-lattice contributions to the diffraction pattern. Red lines, contribution of the near side of the MT. Orange lines, contribution of the far side. **d**, cryo-EM image of a MT copolymerised with Mal3 and its corresponding (mixed AB) diffraction pattern. Blue and green lines show the A-lattice contributions to the diffraction pattern. Blue lines, near side contribution. Green lines, far side contribution. **e, f,** negative stain-EM images of MTs decorated with kinesin. e, pure tubulin MT. f, MT copolymerised with Mal3. The yellow lines highlight the rows of kinesin on the MT walls (see a, b.) **g,** Diffraction pattern of image e. h, Diffraction pattern of image f. **i,** cryo-EM image of a MT copolymerised with Mal3 and its corresponding A-lattice diffraction pattern.

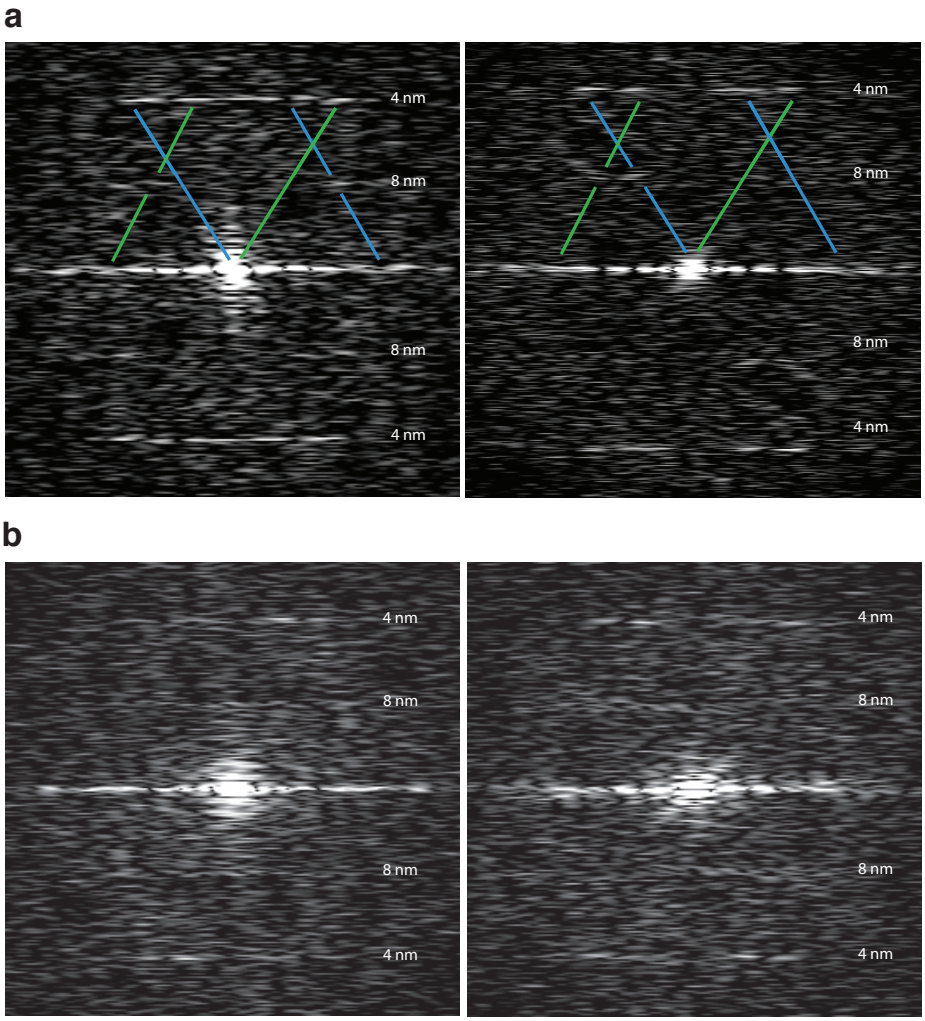

Figure 6.3 Diffraction patterns from brain MTs assembled with Mal3_143
Computed diffraction patterns of cryo-EM image of pig brain MTs copolymerised with Mal3. Blue and green lines show the A-lattice contributions to the diffraction pattern. Blue lines, contribution of the near side of the MT. Green lines, contribution of the far side of the MT. **a:** Pig brain MT diffraction patterns with predominantly A-lattice reflections on the 8nm layerline. **b:** Pig brain MT diffraction patterns with mixed lattice reflections on the 8nm layerline.

It was also fortunate because A-lattice 13 pf MTs are actually truly helical, which allowed the use of helical reconstruction methods. 13 pf MTs are usually thought to not have a super-twist. Without a super-twist, contributions from the back and the front cannot easily be separated. It is manifested in the diffraction pattern by a significant overlap of layerlines from the front and from the back of the tube (see Fig. 6.4).

There is no such problem with 15 pf MTs because their super-twist rotates their reciprocal lattice and as the back and the front lattices rotate in opposite directions, layerlines separate and their respective contributions can be measured directly.

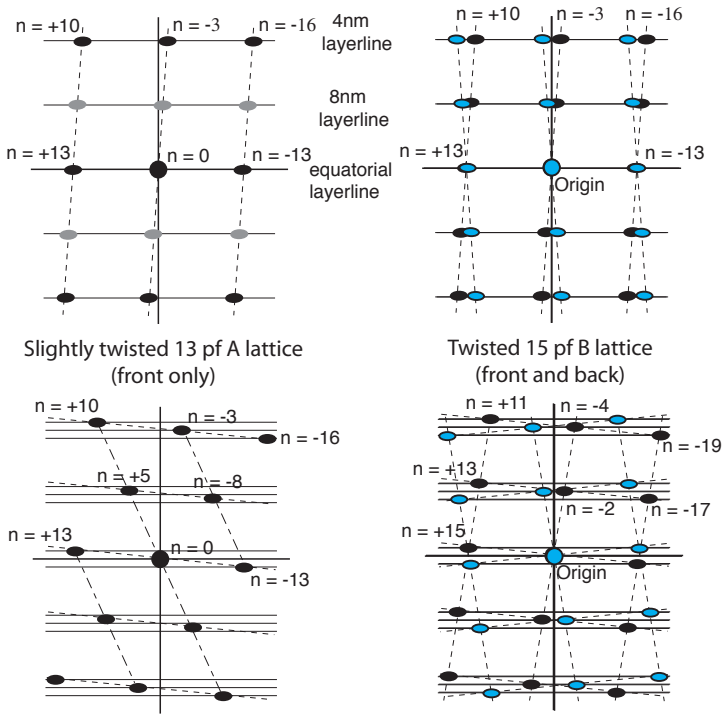

Fig. 6.4 Microtubule reciprocal lattices.
Diffraction patterns from truly helically symmetrical filaments can be indexed according to an appropriate reciprocal lattice. Each peak is indexed according to its n and l number. The Bessel order n is the number of helices in a particular helical family and l is the layerline number. The distance between the first layer and the equator is the reciprocal of the overall longitudinal repeat distance in real space and other layerlines correspond to fractions of that distance. A MT with straight pfs repeats after 8 nm, so l=1 for the 8 nm layerline and l = 2 for the 4 nm layerline.
In the 13 pf B lattice (top left), the spacing of the reflection labeled n = -3 on the 4 nm layer line needs to be halved to make the 8 nm unit cell. In the A lattice (bottom left) it is the one labeled n=10 which is halved, leading to a different 8 nm unit cell from that of the B lattice. Note that half of 3 is not an integer, accounting for the fact that the 13 pf B lattice is not a helical structure when looking at the 8 nm repeat. After 1 turn of the 8 nm dimer helix, it needs to jump by 4nm (at the 'seam') to add the missing half-turn. In the 15 pf B lattice (bottom right) this helical family becomes a 4 start helix family. Therefore, 15 pf B lattice MTs can be true helical structures with 2 perfect dimer helices.
In a transmission image, there are contributions from the two sides of the MT wall. On the left panels are shown only the contributions from the front. On the right, are shown the contributions from the two sides, with the ones from the back shown in blue. For a MT with 13 straight pfs, some contributions from the two sides overlap. When pfs have a helical twist (lower panels) contributions from the two sides are separated and can be measured independently.

3D reconstruction of a 13 pf A-lattice MT decorated with Mal3

Fortuitously, these *pombe* MTs, even though they were 13-protofilament MTs, had a slight super-twist (see Fig. 6.4, bottom right), which allowed analysis of the EM images by helical reconstruction methods. Four MT images out of several hundreds showed diffraction patterns corresponding to a symmetrical A lattice. Layerlines from their diffraction patterns were selected and averaged (Fig. 6.5). Finally, a 3D map at ~2nm resolution was calculated by Fourier-Bessel transformation (Fig. 6.6).

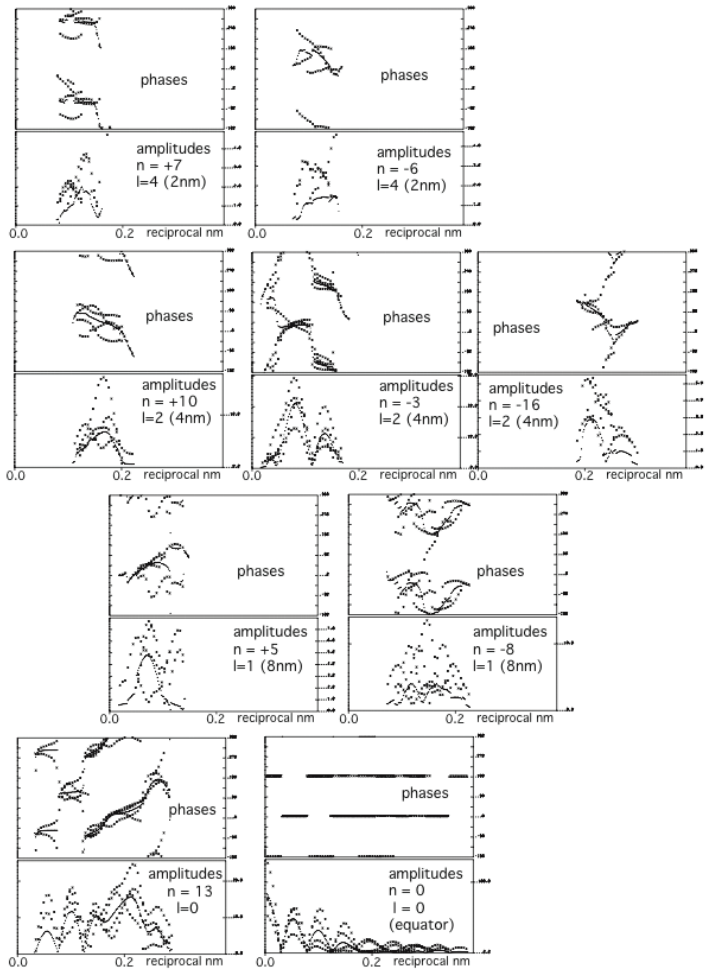

Figure 6.5 Layerline data; Plots of amplitude and phase of the layerlines from 4 different images are superimposed. The Bessel order (n) and layerline number (l) are shown in each plot.

The 3D map of the decorated MT (Fig. 6.6) shows the Mal3 MT binding domain making an extensive contact with one tubulin subunit and occupying the groove between protofilaments. This site is consistent with metal-shadowed EM images showing Mal3 in a similar location (Sandblad et al., 2006). The tubulin subunit making the predominant contact is tentatively assigned as alpha tubulin since an alanine scanning study of *Saccharomyces cerevisiae* alpha tubulin indicated extensive interaction with Bim1C, the *S. cerevisae* homologue of Mal3 (Richards et al., 2000). No contact between Mal3_143 and the neighbouring protofilament is seen at this resolution, but they are sufficiently close that the predominantly unstructured C-terminus of Mal3's MT-binding domain could bridge across, potentially allowing the 3 arginines at the end of this flexible domain to interact with the acidic E-hook (Bhattacharyya, Sackett, &

Wolff, 1985; Sackett & Wolff, 1986) at the C-terminus of a neighbouring tubulin subunit. This would explain why this positively charged region at the end of the flexible linker is so important for microtubule stabilisation (see chapter 5). It would act as a bridging domain, stabilising inter-protofilament contacts and therefore preventing catastrophe events. A much higher resolution, difficult to obtain by EM, would be needed to see directly where this small domain interacts. But maybe, a slightly higher resolution map could provide an indication. Another way to test this hypothesis would be to do a cross-linking experiment followed by mass spectrometry to identify domains of interaction.

It has been shown that MTs polymerised in the presence of high salt have a higher proportion of A lattice interactions (Dias & Milligan, 1999). Mal3's three arginines could have the same effect on the MT lattice as a high salt concentration by quenching the tubulin E-hook negative charges. It has also been shown that MTs treated by subtilisin, which removes the E-hooks, assemble in abnormal fashion (Bhattacharyya et al., 1985). These different results suggest that this highly charged domain has an important role in microtubule formation and maybe in determining lattice geometry. But it remains to be further tested.

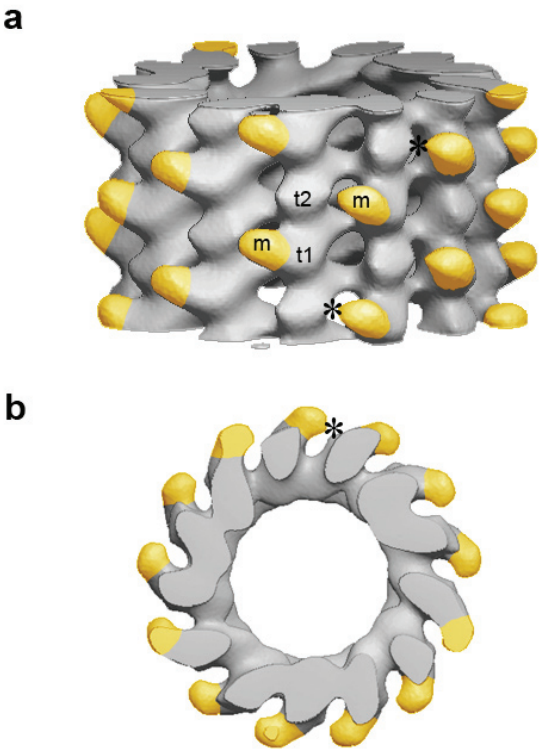

Figure 6.6 3D reconstruction of an A-lattice MT decorated with Mal3_143.
a, Side view of the MT. (+end upwards). **b,** end-on projection seen from the +end. Mal3 density is highlighted in yellow. Asterisks show where Mal3 (m) almost touches a tubulin subunit in the neighbouring protofilament. Subunits t1 and t2 may represent alpha and beta tubulin, respectively.

CHAPTER 7

Cross-linking experiment

Strategy

Since an alanine scanning study of *Saccharomyces cerevisiae* alpha tubulin indicated extensive interaction with Bim1C, the *S. cerevisae* homologue of Mal3 (Richards et al., 2000), the tubulin subunit making the predominant contact was tentatively assigned as α-tubulin. But as the published experiment did not address the role of β-tubulin, it cannot definitely be concluded that only α-tubulin is involved and is actually the main contact. Experiments described here pinpoint the important role of the arginine rich linker for MT stabilisation. This suggests a model mechanism in which the flexible linker region bridges over to the next protofilament and interacts with the acidic E-hook of tubulin. But the 3D image of Mal3 bound to the microtubule is not at high enough resolution to fully validate this model. One way to answer the question may be to use a zero length cross-linker followed by tryptic digestion and mass spectrometry analysis to map the domains of interaction between Mal3 and tubulin.

1-Ethyl-3-[3-dimethylaminopropyl]carbodiimide hydrochloride (EDC or EDAC) is a zero-length crosslinking agent that couples carboxyl groups to primary amines. EDC reacts with a carboxyl to form an amine-reactive O-acylisourea intermediate. If this intermediate does not encounter an amine, it will hydrolyze and regenerate the carboxyl group. If it encounters an amine, it will create a stable amide bond. The different crosslinking products can then be separated by SDS-PAGE, the ones of interest cut out and digested into small peptides by trypsin. Peptides can be analysed by MALDI-TOF

mass spectrometry and cross-linked peptides identified.

Method

10 μM Mal3 was mixed on ice with 5 μM tubulin and 1 mM GTP in BRB80 buffer. Polymerisation was induced by raising the temperature to 30 °C for 30 min. 0.1 mg/ml EDC was added and the solution incubated for 2 hrs. The reaction was quenched by adding 20 mM β-Mercaptoethanol. The solution was then analysed by SDS-PAGE. Protein bands of interest were cut out, the protein extracted and digested with trypsin. The tryptic peptide masses were determined by MALDI mass spectrometry in a PerSeptive Biosystems Voyager-DE STR mass spectrometer using external standards or matrix peaks and trypsin peptides as internal standards. The peptides were identified with MOWSE (Pappin et al., 1993).

Results

The cross-linking experiment between Mal3 full-length and microtubules yielded an important number of bands of variable molecular weight. Some had molecular weights that could correspond to a Mal3-tubulin complex, to a Mal3-Mal3 complex or to a tubulin-tubulin complex. Bands running higher on the SDS-PAGE gel were crosslinked complexes of multiple proteins. Varying the amount of cross-linking agent shifted the ratio between these populations. Less EDC gave an important fraction of free protein and crosslinked protein complexes with a large range of molecular weights. Increasing the amount of EDC shifted the ratio towards high molecular weight specimens. The amount of EDC necessary to have the major part of the protein in solution crosslinked resulted in multiple crosslinks running at very high molecular weights or not running at all on the gel (see Fig. 7.1). The problem with this experiment comes from the number of possible crosslinked species with tubulin in its polymerised microtubule form and

from Mal3 that may also bridge several tubulin subunits and be crosslinked itself by its dimerisation domain. This makes the experiment impossible to fine-tune to get only the species of interest.

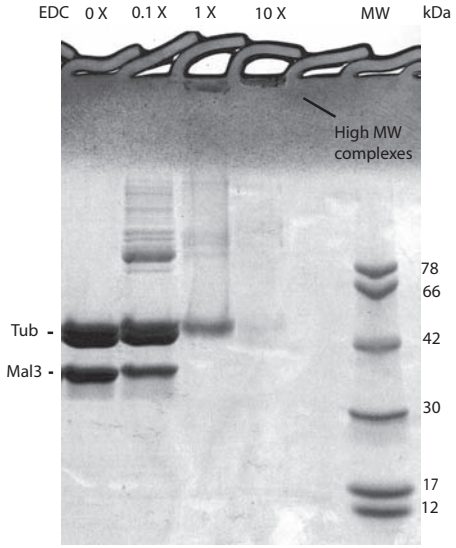

Figure 7.1 Mal3_308 - tubulin crosslinking experiment. EDC was added at different concentrations to a 10 μM solution of Mal3_308 (1 X = 0.1 mg/ml) and incubated for 15 min.
5 μM tubulin with GTP were then added and the temperature raised to 30 ºC to induce polymerisation. The solution was incubated 2 hrs, quenched and loaded on a SDS gel to observe the crosslinking products.

To obtain less very high molecular weight species, the small Mal3_143 construct was used. With the monomer construct, there remains the possibility of having unwanted tubulin-tubulin crosslinks. This experiment gave more homogenous results, with much less very high molecular weight species and some relatively well defined bands corresponding to complexes of only two proteins (Fig. 7.2).

These bands were trypsin digested and analysed by MALDI-TOF and were found to be composed of the 3 proteins: Mal3, α-tubulin and β-tubulin. However, even a careful analysis of the peptide masses did not allow the identification of crosslinked peptides.

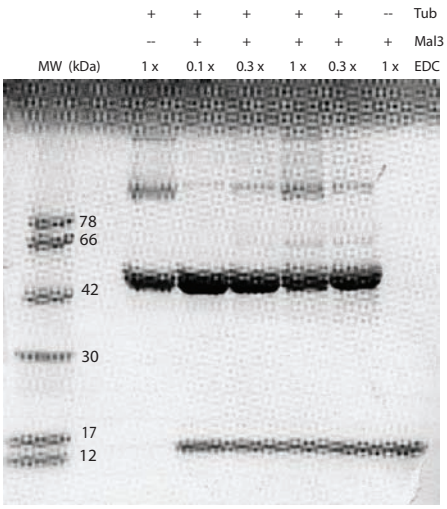

Figure 7.2 Mal3_143 - Tubulin crosslinking experiment.
EDC was added at different concentrations to a 10 µM solution of Mal3_143 (1 X = 0.1 mg/ml) and incubated for 15 min. 5 µM Tubulin with GMPCPP were then added and the temperature raised to 30 ºC to induce polymerisation. The solution was incubated 2 h, quenched and loaded on a SDS-page gel to observe the crosslinking products

There are several ways in which this experiment can be improved in future work to enable identification of crosslinked peptides. The first one is to achieve a better yield of crosslinked products. In the last experiment there was still a major fraction of free protein. It would be important to reduce that fraction to a minimum, without having too much high molecular weight products. Another direction is to obtain more sensitive detection from a better mass spectrometry facility, but this will not be possible in the near future. A third way, which will be tried, is to use mono and deuterated crosslinking agents (BS^3-d_0/d_4 and BS^2G-d_0/d_4, Pierce), which when mixed in equal proportions will crosslink peptides equally. Crosslinked peptides will be much easier to detect by mass spectrometry because they will be the only peaks of equal height with a difference in mass of exactly two Daltons. This work will be done after this thesis is submitted.

Another way to reach a more precise understanding of the Mal3 binding site on the microtubule is to calculate a higher resolution electron density map, which would enable a precise docking of the MT binding domain and eventually visualise the connection made by the linker domain. With this objective in mind, Mal3 crystallization was attempted, as described in the next Chapter.

CHAPTER 8

Mal3 X-ray crystallographic Study

Strategy

To obtain additional information on Mal3 architecture, attempts were made to crystallize the full-length protein. As it is very likely that it has a very flexible domain organisation, attempts were also made on the microtubule-binding domain alone, with various lengths of the putative flexible linker.

Methods

Initial Mal3 crystallization conditions were found from a 1440 condition screen set up using a high-throughput nanolitre robotic system (Stock, Perisic, & Lowe, 2005). Mal3_308, Mal3_143 and Mal3_125 were crystallised by sitting drop vapour diffusion against mother liquors described in Figures 8.1, 8.2 and 8.3. Artificial mother liquor mixed with 30 % glycerol as cryoprotectant was added directly to the Mal3_125 drop before crystals were flash frozen in liquid nitrogen. Mal3_125 crystals grew in the monoclinic space group C121 with cell dimensions a = 58.1 Å, b = 67.4 Å, c = 62.2 Å, $\beta = 91.9°$. Datasets collected on Mar 2000 were integrated using MOSFLM (Leslie, 1992) and reduced using SCALA (CCP4 1994; Evans, 2006). Crystals were solved by molecular replacement using PHASER (Read, 2001) with the model of the EB1 CH domain solved by Hayashi and Hikura (Hayashi & Ikura, 2003). Refinement is currently being performed using CNS version 1.1 with Engh and Huber stereochemical parameters (Engh & Huber, 1991) or REFMAC 5.2 (Murshudov, Vagin, & Dodson,

1997) and manual model building is being performed using MAIN2003 (Turk, 1992).

Results

Mal3 full length gave crystals in 30% PEG4000, 0,1 M Tris pH 8.5, 02 M lithium sulphate (Fig. 8.1) but these tiny needles could never be reproduced. It is very likely that the protein's intrinsic flexibility impedes it from making regular crystalline arrangements and seeing crystals in one set of conditions was a great surprise. It was a shame that attempts to reproduce these crystals failed. Crystallising the MT binding domain alone should be easier as it removes the dimerisation domain, which is thought to be flexibly linked to the MT binding domain.

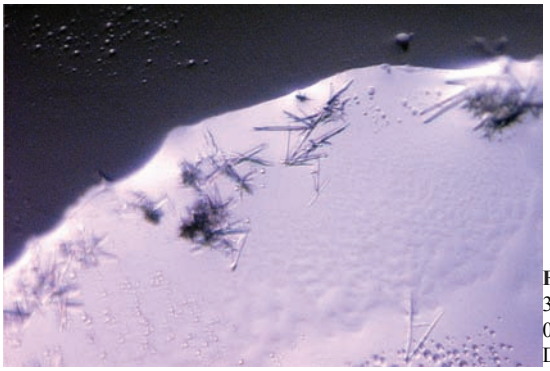

Figure 8.1 Mal3_308 crystals. 30% PEG4000, 0,1 M Tris pH 8.5, 02 M lithium sulphate (plate lmb 8 D9). Never reproduced.

Indeed, the construct Mal_143 crystallised in tiny needles, often forming clusters. The same crystal form was observed in several different conditions (see Fig. 8.2) Attempts to optimize this crystal form, in particular trying to obtain monocrystals instead of numerous needles, did not yield any success (Fig. 8.2). It did give some slightly bigger needles, but still far too small to be put under an X-ray beam. The problem was very likely due to the remaining flexible linker, which might still cause problems to the crystallisation.

Figure 8.2 Mal3 143 crystallization trials.
Initial screen. A. 2M ammonium sulphate. Clusters with tiny needles. **Optimization: B.** 3.5 M ammonium sulphate, 0,1 M citric acid pH4. **Additive screen: C.** 1.5 ammonium sulphate, 0.1 M citric acid, pH 4, 0,01 M cadmium chloride hydrate. **D.** 1.5 ammonium sulphate, 0.1 M citric acid, pH 4, 0.2 M NDSB 211.

Removing the entire flexible linker greatly improved crystallisation. The construct Mal3_125 crystallised under many different sets of conditions (Fig. 8.3) and immediately diffracted to 1.8 Angstroms in-house. The first crystal died by accident but the second crystal gave a complete dataset at 2.0 Angstroms on Mar 2000 (see Table 8.1). Existence of the Mal3 homologue EB1 CH domain crystal structure gave the possibility to solve the structure by molecular replacement. The structure still needs to be fully built and refined. This work will be completed after thesis submission, along with efforts to improve the EM map resolution for a precise docking.

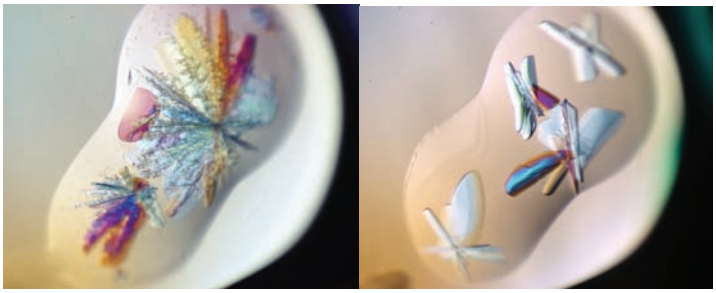

Figure 8.3 Mal3_125 crystallization screen.
Right: 1.8 M sodium/potassium phosphate pH 7.5
Left:: 1.8 M sodium/potassium phosphate pH 8.2.
Crystals from the left drop diffract to 1.8 Å resolution on a Mar2000 X-ray generator.

Table 8.1 Crystallographic data Mal3_125

Unit cell: C121, a = 58.1 Å, b = 67.4 Å, c = 62.2 Å, β= 91.9°

Crystal	λ[Å]	resol.	I/σI1	Rm[2][%]	multipl.[3]	Compl.[%][4]
mal125_lmb3f12b	1.54	2 Å	8.2 (1.9)	0.075 (0.364)	3.3 (3.2)	99.5 (99.5)

[1]signal to noise ratio for merged intensities (highest resolution bins in brackets). [2]Rm: ΣhΣi|I(h,i)-I(h)| / ΣhΣi I(h,i) where I(h,i) are symmetry related intensities and I(h) is the mean intensity of the reflection with unique index h. [3]Multiplicity for unique reflections (highest resolution bins in brackets).
[4]Completeness for unique reflections.

CHAPTER 9

Discussion and future directions

The original aim of characterising the whole +Tip complex was not achieved, as the pull-down experiment did not give a full complex and as recombinant Tip1 and Tea2 proved difficult to express and purify from *E. coli*. Tip1 had cleavage problems and Tea2 has been expressed but only in a truncated form, the full length form being poorly soluble. Much more work will have to be done to circumvent these problems and reconstitute the full complex. It is still an important goal but work on Mal3 alone proved so interesting that experiments on Tip1 and Tea2 were set aside.

The biochemical and structural data gathered for Mal3 interaction with tubulin favours a model in which Mal3 monomer domains stabilize MTs by bridging tubulin subunits on adjacent protofilaments. The first evidence comes from the importance of the flexible linker domain and its arginine rich cluster. It is a very good candidate for interacting with one or both of the tubulin C-terminal acidic tails. Such an interaction is likely to occur on a different subunit from the one to which the main MT binding domain is bound, therefore making a bridging bond. The structural data, showing Mal3 MT binding domain making an extensive contact on one tubulin subunit and being oriented towards the groove between protofilaments, very close to the neighbouring tubulin subunit, reinforce this hypothesis. Also, Mal3 has only been found to interact to MTs and not to tubulin in solution. Mal3 binding site must therefore only be present on a tubulin polymer. The fact that Mal3 promotes MT nucleation means that it must stabilize small tubulin polymers in the early stages of assembly. Tubulin in such polymers must

have a very similar conformation to free tubulin in solution. If Mal3 binds to these early polymers, it is very unlikely that a particular tubulin conformation prevents Mal3 from binding to tubulin in solution. Therefore, it is very unlikely that Mal3 has an influence on tubulin conformation. Otherwise it would immediately modify tubulin assembly kinetic parameters as well. This also points that Mal3 may needs the additional binding site made by tubulin polymers. And by bridging adjacent tubulin subunits, Mal3 stabilizes transient tubulin polymers and favours MT nucleation.

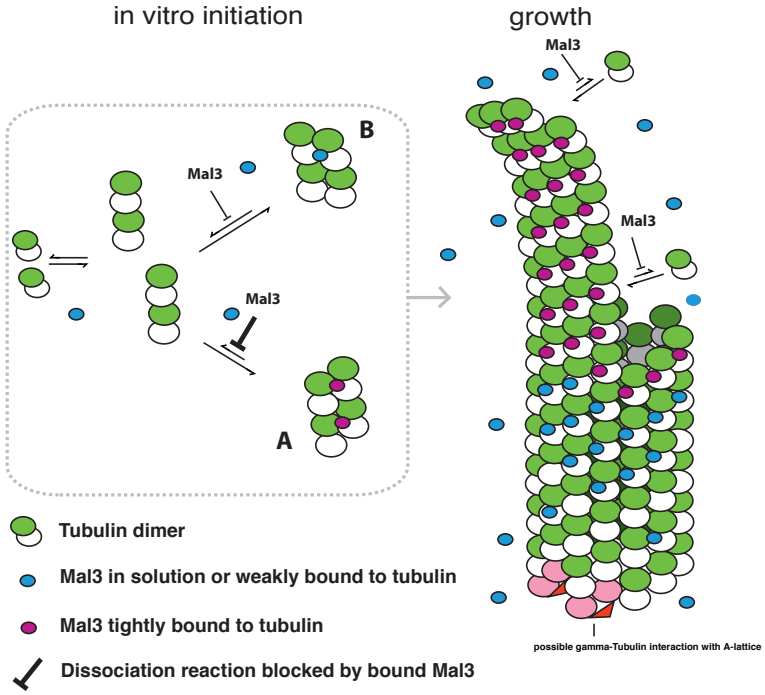

Figure 9.1 Model of how Mal3 may promote assembly of A-lattice MTs. White subunits, alpha-tubulin. Green subunits, beta-tubulin. Stably bound Mal3 monomers in magenta. More weakly bound Mal3 in Blue. In vitro tubulin heterodimers will form oligomers that may either continue to assemble or may dissociate again. We propose that Mal3 binds to and stabilises A oligomers better than B oligomers, thus promoting their growth into larger complexes and seeding a future MT with a high proportion of A-lattice contacts. As a MT grows, Mal3 binds tightly to the tip, which might correspond to an extension with a similar structure to the oligomer seeds. Mal3 binds only weakly to the closed MT lattice. γ-tubulin complexes (pink and red) (Kollman et al. 2008, Moritz et al. 2000) may initiate pure A-lattice assembly in vivo by interacting with both alpha and beta-tubulin (Oakley & Oakley, 1989).

The data presented here and by Sandblad et al. (2006) show that Mal3 binds better to an A-lattice than to a B-lattice. This could be due to two factors: a different binding site or a different availability of part of the binding site because of the staggered arrangement (Fig. 6.6). In a staggered arrangement, an α-tubulin interacts with a β-tubulin from the next protofilament. With a B-lattice, it would interact with another α-tubulin. Therefore, if Mal3 interacts with tubulin subunits on two protofilaments, the binding site will be different depending on the lattice arrangement. The second factor could be that in a B-lattice arrangement, the binding of another Mal3 on the adjacent tubulin subunit could

mask part of the binding site. This would weaken the affinity and at the same time might suppress the possibility for the poly-arginine linker of the first molecule to bridge the two protofilaments. As a result, the stabilization activity would not exist. This would readily explain why Mal3 favours the formation of A-lattice MTs. With an A-lattice staggered arrangement, the adjacent tubulin subunit would always be free to interact with the flexible poly-arginine linker. Stabilization would therefore be much greater.
The free binding site made by the staggered arrangement alone would not explain why on a sparsely populated MT surface Mal3 is seen to bind only along the seam. On an unsaturated MT, where there is no competition for binding sites and the staggered arrangement would not make a difference, only a difference in binding site would explain this behaviour. Overall a composite of these two factors would best explain all my observations. The A-lattice staggered arrangement, where there is no binding site overlaps between different Mal3 proteins, explains well why Mal3 stabilizes better A-lattice MTs. It can also explain a better binding to the MT lattice but in conjunction with the different binding site that the A-lattice provides.

This still does not explain why Mal3 binds at the growing end of MTs with higher affinity. Is it a different conformation such as the sheet structure or an available binding site masked afterwards? Or is it simply the presence of GTP tubulin at the tip of growing MTs making Mal3 binds stronger? The 8s time-lapse before Mal3 fades from the MT wall seems to be in favour of this last hypothesis (Bieling et al., 2007). But why do we not observe a better binding with GMPCPP by pelleting assay? Does GMPCPP give tubulin a slightly different conformation from GTP so that Mal3 binds with a different affinity to the two structures? The pelletting assay may not be sensitive enough to see that difference. An interesting way to test that idea would be to repeat the Bieling et al. experiment with GMPCPP added at a certain time and see if it changes Mal3 binding profile.

Now it is necessary to ask what is the significance of the discovery that Mal3 enhances the proportion of A-lattice assemblies in vitro? Does it reflect the in vivo MT lattice or is it simply an in vitro artefact? One could argue that Mal3 function may actually be the one suggested by Sandblad et al. and Vitré et al.: namely that Mal3 binds specifically to the seam and acts as a molecular zipper on the supposedly weak part of the MT structure. Until the actual in vivo MT structure is defined, this hypothesis will stay on hold. Also, the finding that Mal3 needs to be in a stoichiometric ratio with tubulin to fully shift it towards its polymerised form in vitro does not fit with a model where it would only be needed to stabilize the seam. Now, in vivo, Mal3 may not be able to influence the MT lattice, which must be fixed initially by the MT nucleation centres such as the gamma-tubulin ring complex. MTs almost never nucleate de novo at random places in the cytoplasm. If the MT lattice nucleated by gamma-tubulin ring complexes were the A-lattice, Mal3 could be part of the regulatory mechanism which promotes MT growth only from the MTOC. MTs nucleating from any random place might have the B-lattice and therefore not be efficiently stabilized by Mal3. As EB1 family proteins are ubiquitous among eukaryotes, such a function could be common to all eukaryotes.
One could also argue that a truly helical lattice makes more sense than a lattice having to bear a discontinuity. The first model of the flagellar outer doublet, with the complete A tubule having a truly helical A-lattice and the B-tubule, which is not complete and therefore does not need to be helical, having a B-lattice makes a lot of sense. It is also an efficient way to make a distinction between these two tubules and to associate them with the different sets of proteins that are actually observed at their surface (Hoops & Witman, 1983; Nicastro et al., 2006; Satir & Christensen, 2008).
Two different lattices for different sets of functions is actually a very likely hypothesis. The two sets of lateral contacts ($\alpha\ \alpha$, $\beta\ \beta$ and $\alpha\ \beta$, $\beta\ \alpha$) have been conserved among all eukaryotes. These two sets of interfaces could not be conserved if they were not used in

all eukaryotic species. As they are both present on a B-lattice MT with a seam, it means that the B-lattice must exist. And as the B-lattice MT can explain it all, existence of the A-lattice MT may not be required to explain the conservation of A-lattice contacts. It does not rule it out either. The many MT related functions would certainly be beneficial of the possibility of having two different MT lattices. The flagellar outer doublet is the most obvious one. We could also imagine that interphase MTs are stabilized A-lattice MTs whereas much more dynamic mitosis MTs may have a B-lattice and a different set of associated proteins. Some cell types are also found to have different sets of MTs, some being more dynamic than others. For example, dendritic MTs are more dynamic than the core of axonal MTs. In some cell types, different MT populations are also found to have different states of tyrosination or other post-translational modifications. It is difficult to explain how the cell produces these different sets of MTs. Having two sets of MTs with two different lattices to attract different proteins would be an interesting possibility.

The most tangible point in favour of the in vivo existence of the A-lattice is the finding by Oakley and Oakley that gamma-tubulin interacts physically with β-tubulin (Oakley & Oakley, 1989). Such contact could only occur if an A-lattice MT was nucleated from the gamma-tubulin ring complex. Moritz et al. have made a 3D reconstruction of the γ-TuRC by cryo-EM. They attempted to draw a model of how such a complex could serve as template for a B-lattice MT. But looking at the γ-TuRC image, it seems able to accommodate a staggered MT just as well, if not better. Defining which lattice is actually nucleated from these γ-TuRCs might give a very important clue on which lattice is actually present in the cell. I will do my best to get an answer as soon as this thesis is submitted.

Indeed, defining which lattice is present in the cell is a very important question as

many cellular processes might be influenced by it. As discussed above, different sets of proteins and functions might be associated to different MT lattices. But also, it has to be said that all the biochemical work done until today with MTs has been done with in vitro assembled B-lattice MTs, often Taxol stabilized. A lot of these biochemical data would have to be reassessed if it appeared that the canonical lattice was the A-lattice. Many MAPs might have very different behaviour and binding properties on an A-lattice MT compared to what has been observed until today. Kinesins might be able to make 4nm sideways steps on an A-lattice MT, instead of walking straight by 8 nm steps on a single protofilament. Who knows?…

References

Akhmanova, A. & Hoogenraad, C. C. (2005). Microtubule plus-end-tracking proteins: mechanisms and functions. *Curr Opin Cell Biol*, *17*(1), 47-54.

Allen, C. & Borisy, G. G. (1974). Structural polarity and directional growth of microtubules of Chlamydomonas flagella. *J Mol Biol*, *90*(2), 381-402.

Amos, L. & Klug, A. (1974). Arrangement of subunits in flagellar microtubules. *Journal of Cell Science*, *14*(3), 523-549.

Arnal, I., Heichette, C., Diamantopoulos, G. S., & Chrétien, D. (2004). CLIP-170/tubulin-curved oligomers coassemble at microtubule ends and promote rescues. *Curr Biol*, *14*(23), 2086-2095.

Bahler, J., Wu, J. Q., Longtine, M. S., Shah, N. G., McKenzie, A. r., Steever, A. B. et al. (1998). Heterologous modules for efficient and versatile PCR-based gene targeting in Schizosaccharomyces pombe. *Yeast*, *14*(10), 943-951.

Behrens, R. & Nurse, P. (2002). Roles of fission yeast tea1p in the localization of polarity factors and in organizing the microtubular cytoskeleton. *J Cell Biol*, *157*(5), 783-793.

Beinhauer, J. D., Hagan, I. M., Hegemann, J. H., & Fleig, U. (1997). Mal3, the fission yeast homologue of the human APC-interacting protein EB-1 is required for microtubule integrity and the maintenance of cell form. *J Cell Biol*, *139*(3), 717-728.

Bhattacharyya, B., Sackett, D. L., & Wolff, J. (1985). Tubulin, hybrid dimers, and tubulin S. Stepwise charge reduction and polymerization. *J Biol Chem*, *260*(18), 10208-10216.

Bieling, P., Laan, L., Schek, H., Munteanu, E. L., Sandblad, L., Dogterom, M. et al. (2007). Reconstitution of a microtubule plus-end tracking system in vitro. *Nature*, *450*(7172), 1100-1105.

Bridge, A. J., Morphew, M., Bartlett, R., & Hagan, I. M. (1998). The fission yeast SPB component Cut12 links bipolar spindle formation to mitotic control. *Genes Dev*, *12*(7), 927-942.

Browning, H., Hayles, J., Mata, J., Aveline, L., Nurse, P., & McIntosh, J. R. (2000). Tea2p is a kinesin-like protein required to generate polarized growth in fission yeast. *J Cell Biol*, *151*(1), 15-28.

Browning, H. & Hackney, D. D. (2005). The EB1 homolog Mal3 stimulates the ATPase of the kinesin Tea2 by recruiting it to the microtubule. *J Biol Chem*, *280*(13), 12299-12304.

Browning, H., Hackney, D. D., & Nurse, P. (2003). Targeted movement of cell end factors in fission yeast. *Nat Cell Biol*, *5*(9), 812-818.

Brunner, D. & Nurse, P. (2000). CLIP170-like tip1p spatially organizes microtubular dynamics in fission yeast. *Cell*, *102*(5), 695-704.

Busch, K. E. & Brunner, D. (2004). The microtubule plus end-tracking proteins mal3p and tip1p cooperate for cell-end targeting of interphase microtubules. *Curr Biol*, *14*(7), 548-559.

Busch, K. E., Hayles, J., Nurse, P., & Brunner, D. (2004). Tea2p kinesin is involved in spatial microtubule organization by transporting tip1p on microtubules. *Dev Cell*, *6*(6), 831-843.

Carvalho, P., Gupta, M. L. J., Hoyt, M. A., & Pellman, D. (2004). Cell cycle control of kinesin-mediated transport of Bik1 (CLIP-170) regulates microtubule stability and dynein activation. *Dev Cell*, *6*(6), 815-829.

Castoldi, M. & Popov, A. V. (2003). Purification of brain tubulin through two cycles of polymerization-depolymerization in a high-molarity buffer. *Protein Expr Purif*, *32*(1), 83-88.

Chrétien, D. & Fuller, S. D. (2000). Microtubules switch occasionally into unfavorable configurations during elongation. *J Mol Biol*, *298*(4), 663-676.

Chrétien, D., Fuller, S. D., & Karsenti, E. (1995). Structure of growing microtubule ends: two-dimensional sheets close into tubes at variable rates. *J. Cell Biol*, *129*(5), 1311-1328.

Crowther, R. A., Henderson, R., & Smith, J. M. (1996). MRC image processing programs. *J Struct Biol*, *116*(1), 9-16.

Davis, A., Sage, C. R., Wilson, L., & Farrell, K. W. (1993). Purification and biochemical characterization of tubulin from the budding yeast Saccharomyces cerevisiae. *Biochemistry*, *32*(34), 8823-8835.

Desai, A., Verma, S., Mitchison, T. J., & Walczak, C. E. (1999). Kin I kinesins are microtubule-destabilizing enzymes. *Cell*, *96*(1), 69-78.

Desai, A. & Mitchison, T. J. (1997). Microtubule polymerization dynamics. *Annu Rev Cell Dev Biol*, *13*, 83-117.

Diamantopoulos, G. S., Perez, F., Goodson, H. V., Batelier, G., Melki, R., Kreis, T. E. et al. (1999). Dynamic localization of CLIP-170 to microtubule plus ends is coupled to microtubule assembly. *J Cell Biol*, *144*(1), 99-112.

Dias, D. P. & Milligan, R. A. (1999). Motor protein decoration of microtubules grown in high salt conditions reveals the presence of mixed lattices. *J Mol Biol*, *287*(2), 287-292.

Drechsel, D. N. & Kirschner, M. W. (1994). The minimum GTP cap required to stabilize microtubules. *Current Biology*, *4*(12), 1053-1061.

Engh, R. A. & Huber, R. (1991). {Accurate bond and angle parameters for X-ray protein structure refinement. *Acta Crystallographica Section A*, *47*(4), 392–400.

Evans, P. (2006). Scaling and assessment of data quality. *Acta Crystallogr D Biol Crystallogr*, *62*(Pt 1), 72-82.

Folker, E. S., Baker, B. M., & Goodson, H. V. (2005). Interactions between CLIP-170, tubulin, and microtubules: implications for the mechanism of Clip-170 plus-end tracking behavior. *Mol Biol Cell*, *16*(11), 5373-5384.

Grandi, P., Doye, V., & Hurt, E. C. (1993). Purification of NSP1 reveals complex formation with 'GLFG' nucleoporins and a novel nuclear pore protein NIC96. *EMBO J*, *12*(8), 3061-3071.

Hayashi, I. & Ikura, M. (2003). Crystal structure of the amino-terminal microtubule-binding domain of end-binding protein 1 (EB1). *J Biol Chem*, *278*(38), 36430-36434.

Honnappa, S., John, C. M., Kostrewa, D., Winkler, F. K., & Steinmetz, M. O. (2005). Structural insights into the EB1-APC interaction. *Embo J*, *24*(2), 261-269.

Hoops, H. J. & Witman, G. B. (1983). Outer doublet heterogeneity reveals structural polarity related to beat direction in Chlamydomonas flagella. *J Cell Biol*, *97*(3), 902-908.

Hyman, A. A., Salser, S., Drechsel, D. N., Unwin, N., & Mitchison, T. J. (1992). Role of GTP hydrolysis in microtubule dynamics: information from a slowly hydrolyzable analogue, GMPCPP. *Mol Biol Cell*, *3*(10), 1155-1167.

Hyman, A. A., Chrétien, D., Arnal, I., & Wade, R. H. (1995). Structural changes accompanying GTP hydrolysis in microtubules: information from a slowly hydrolyzable analogue guanylyl-(alpha,beta)-methylene-diphosphonate. *J Cell Biol*, *128*(1-2), 117-125.

Janosi, I. M., Chrétien, D., & Flyvbjerg, H. (2002). Structural microtubule cap: stability, catastrophe, rescue, and third state. *Biophys J*, *83*(3), 1317-1330.

Kar, S., Fan, J., Smith, M. J., Goedert, M., & Amos, L. A. (2003). Repeat motifs of tau bind to the insides of microtubules in the absence of taxol. *EMBO J*, *22*(1), 70-77.

Keeney, J. B. & Boeke, J. D. (1994). Efficient targeted integration at leu1-32 and ura4-294 in Schizosaccharomyces pombe. *Genetics*, *136*(3), 849-856.

Kinoshita, K., Arnal, I., Desai, A., Drechsel, D. N., & Hyman, A. A. (2001). Reconstitution of physiological microtubule dynamics using purified

components. *Science*, *294*(5545), 1340-1343.

Knop, M. & Schiebel, E. (1997). Spc98p and Spc97p of the yeast gamma-tubulin complex mediate binding to the spindle pole body via their interaction with Spc110p. *EMBO J*, *16*(23), 6985-6995.

Kollman, J. M. et al. The Structure of the gamma-Tubulin Small Complex: Implications of Its Architecture and Flexibility for Microtubule Nucleation. Mol. Biol. Cell 19, 207-215 (2008).

Krylyshkina, O., Kaverina, I., Kranewitter, W., Steffen, W., Alonso, M. C., Cross, R. A. et al. (2002). Modulation of substrate adhesion dynamics via microtubule targeting requires kinesin-1. *J Cell Biol*, *156*(2), 349-359.

Lansbergen, G. & Akhmanova, A. (2006). Microtubule plus end: a hub of cellular activities. *Traffic*, *7*(5), 499-507.

Lansbergen, G., Komarova, Y., Modesti, M., Wyman, C., Hoogenraad, C. C., Goodson, H. V. et al. (2004). Conformational changes in CLIP-170 regulate its binding to microtubules and dynactin localization. *J Cell Biol*, *166*(7), 1003-1014.

Leslie, A. G. W. (1992). Recent changes to the MOSFLM package for processing film and image plate data. *Joint CCP4 + ESF-EAMCB Newsletter on Joint CCP4 + ESF-EAMCB Newsletter on Protein Crystallography, No. 26*.

Lupas, A., Van Dyke, M., & Stock, J. (1991). Predicting coiled coils from protein sequences. *Science*, *252*(5009), 1162-1164.

Manna, T., Honnappa, S., Steinmetz, M. O., & Wilson, L. (2008). Suppression of microtubule dynamic instability by the +TIP protein EB1 and its modulation by the CAP-Gly domain of p150glued. *Biochemistry*, *47*(2), 779-786.

Mata, J. & Nurse, P. (1997). tea1 and the microtubular cytoskeleton are important for generating global spatial order within the fission yeast cell. *Cell*, *89*(6), 939-949.

Mimori-Kiyosue, Y. & Tsukita, S. (2003). “Search-and-capture” of microtubules

through plus-end-binding proteins (+TIPs). *J Biochem*, *134*(3), 321-326.

Mitchison, T. & Kirschner, M. (1984). Dynamic instability of microtubule growth. *Nature*, *312*(5991), 237-242.

Moks, T., Abrahmsen, L., Holmgren, E., Bilich, M., Olsson, A., Uhlen, M. et al. (1987). Expression of human insulin-like growth factor I in bacteria: use of optimized gene fusion vectors to facilitate protein purification. *Biochemistry*, *26*(17), 5239-5244.

Moore, A. T., Rankin, K. E., von Dassow, G., Peris, L., Wagenbach, M., Ovechkina, Y. et al. (2005). MCAK associates with the tips of polymerizing microtubules. *J Cell Biol*, *169*(3), 391-397.

Moores, C. A., Perderiset, M., Francis, F., Chelly, J., Houdusse, A., & Milligan, R. A. (2004). Mechanism of microtubule stabilization by doublecortin. *Mol Cell*, *14*(6), 833-839.

Moreno, S., Klar, A., & Nurse, P. (1991). Molecular genetic analysis of fission yeast Schizosaccharomyces pombe. *Methods Enzymol*, *194*, 795-823.

Moritz, M., Braunfeld, M. B., Guenebaut, V., Heuser, J. & Agard, D. A. Structure of the gamma-tubulin ring complex: a template for microtubule nucleation. Nat Cell Biol 2, 365-370 (2000).

Moritz, M., Zheng, Y., Alberts, B. M., & Oegema, K. (1998). Recruitment of the gamma-tubulin ring complex to Drosophila salt-stripped centrosome scaffolds. *J Cell Biol*, *142*(3), 775-786.

Murshudov, G. N., Vagin, A. A., & Dodson, E. J. (1997). Refinement of macromolecular structures by the maximum-likelihood method. *Acta Crystallogr D Biol Crystallogr*, *53*(Pt 3), 240-255.

Nicastro, D., Schwartz, C., Pierson, J., Gaudette, R., Porter, M. E., & McIntosh, J. R. (2006). The molecular architecture of axonemes revealed by cryoelectron tomography. *Science*, *313*(5789), 944-948.

Nogales, E., Whittaker, M., Milligan, R. A., & Downing, K. H. (1999). High-resolution model of the microtubule. *Cell*, *96*(1), 79-88.

Nogales, E., Wolf, S. G., & Downing, K. H. (1998). Structure of the alpha beta tubulin dimer by electron crystallography. *Nature*, *391*(6663), 199-203.

Oakley, C. E. & Oakley, B. R. (1989). Identification of [gamma]-tubulin, a new member of the tubulin superfamily encoded by mipA gene of Aspergillus nidulans. *Nature*, *338*(6217), 662-664.

Pappin, D. J., Hojrup, P., & Bleasby, A. J. (1993). Rapid identification of proteins by peptide-mass fingerprinting. *Curr Biol*, *3*(6), 327-332.

Peris, L., Thery, M., Faure, J., Saoudi, Y., Lafanechere, L., Chilton, J. K. et al. (2006). Tubulin tyrosination is a major factor affecting the recruitment of CAP-Gly proteins at microtubule plus ends. *J Cell Biol*, *174*(6), 839-849.

Popov, A. V. & Karsenti, E. (2003). Stu2p and XMAP215: turncoat microtubule-associated proteins? *Trends Cell Biol*, *13*(11), 547-550.

Ravelli, R. B., Gigant, B., Curmi, P. A., Jourdain, I., Lachkar, S., Sobel, A. et al. (2004). Insight into tubulin regulation from a complex with colchicine and a stathmin-like domain. *Nature*, *428*(6979), 198-202.

Read, R. J. (2001). Pushing the boundaries of molecular replacement with maximum likelihood. *Acta Crystallogr D Biol Crystallogr*, *57*(Pt 10), 1373-1382.

Richards, K. L., Anders, K. R., Nogales, E., Schwartz, K., Downing, K. H., & Botstein, D. (2000). Structure-function relationships in yeast tubulins. *Mol Biol Cell*, *11*(5), 1887-1903.

Sackett, D. L. & Wolff, J. (1986). Proteolysis of tubulin and the substructure of the tubulin dimer. *J. Biol. Chem*, *261*(19), 9070-9076.

Sandblad, L., Busch, K. E., Tittmann, P., Gross, H., Brunner, D., & Hoenger, A. (2006). The Schizosaccharomyces pombe EB1 homolog Mal3p binds and stabilizes the microtubule lattice seam. *Cell*, *127*(7), 1415-1424.

Satir, P. & Christensen, S. T. (2008). Structure and function of mammalian cilia. *Histochem Cell Biol*, *129*(6), 687-693.

Schuyler, S. C. & Pellman, D. (2001). Microtubule "plus-end-tracking proteins": The end is just the beginning. *Cell*, *105*(4), 421-424.

Slep, K. C. & Vale, R. D. (2007). Structural basis of microtubule plus end tracking by XMAP215, CLIP-170, and EB1. *Mol Cell*, *27*(6), 976-991.

Song, Y. H. & Mandelkow, E. (1993). Recombinant kinesin motor domain binds to beta-tubulin and decorates microtubules with a B surface lattice. *Proc Natl Acad Sci U S A*, *90*(5), 1671-1675.

Song, Y. H. & Mandelkow, E. (1995). The anatomy of flagellar microtubules: polarity, seam, junctions, and lattice. *J Cell Biol*, *128*(1-2), 81-94.

Spittle, C., Charrasse, S., Larroque, C., & Cassimeris, L. (2000). The interaction of TOGp with microtubules and tubulin. *J Biol Chem*, *275*(27), 20748-20753.

Stearns, T. & Kirschner, M. (1994). In vitro reconstitution of centrosome assembly and function: the central role of gamma-tubulin. *Cell*, *76*(4), 623-637.

Stirling, D. A., Petrie, A., Pulford, D. J., Paterson, D. T., & Stark, M. J. (1992). Protein A-calmodulin fusions: a novel approach for investigating calmodulin function in yeast. *Mol Microbiol*, *6*(6), 703-713.

Stock, D., Perisic, O., & Lowe, J. (2005). Robotic nanolitre protein crystallisation at the MRC Laboratory of Molecular Biology. *Prog Biophys Mol Biol*, *88*(3), 311-327.

(1994). The CCP4 suite: programs for protein crystallography. *Acta Crystallogr D Biol Crystallogr*, *50*(Pt 5), 760-763.

Turk, D. (1992). Weiterentwicklung eines Programms fur Molekulgraphik und Elecktronendichte-Manipulation und seine Anwendeing auf verschiedene Protein-Strukturaufklarungen. *Technische Universität München, München, Germany*.

Vaughan, P. S., Miura, P., Henderson, M., Byrne, B., & Vaughan, K. T. (2002). A role for regulated binding of p150(Glued) to microtubule plus ends in organelle transport. *J Cell Biol*, *158*(2), 305-319.

Vitre, B., Coquelle, F. M., Heichette, C., Garnier, C., Chrétien, D., & Arnal, I. (2008). EB1 regulates microtubule dynamics and tubulin sheet closure in vitro. *Nat Cell Biol*, *10*(4), 415-421.

Walker, R. A., O'Brien, E. T., Pryer, N. K., Soboeiro, M. F., Voter, W. A., Erickson, H. P. et al. (1988). Dynamic instability of individual microtubules analyzed by video light microscopy: rate constants and transition frequencies. *J Cell Biol*, *107*(4), 1437-1448.

Wigge, P. A., Jensen, O. N., Holmes, S., Soues, S., Mann, M., & Kilmartin, J. V. (1998). Analysis of the Saccharomyces spindle pole by matrix-assisted laser desorption/ionization (MALDI) mass spectrometry. *J Cell Biol*, *141*(4), 967-977.

Wigge, P. A. & Kilmartin, J. V. (2001). The Ndc80p complex from Saccharomyces cerevisiae contains conserved centromere components and has a function in chromosome segregation. *J Cell Biol*, *152*(2), 349-360.

Zheng, Y., Wong, M. L., Alberts, B., & Mitchison, T. (1995). Nucleation of microtubule assembly by a gamma-tubulin-containing ring complex. *Nature*, *378*(6557), 578-583.